Modulations in the Leading Edges of Midlatitude Storm Tracks

R. H. Goodman; A. J. Majda; D. W. McLaughlin

MODULATIONS IN THE LEADING EDGES OF MIDLATITUDE STORM TRACKS[*]

R. H. GOODMAN[†], A. J. MAJDA[‡], AND D. W. MCLAUGHLIN[‡]

Abstract. Downstream development is a term encompassing a variety of effects relating to the propagation of storm systems at midlatitude. We investigate a mechanism behind downstream development and study how wave propagation is affected by varying several physical parameters. We then develop a multiple scales modulation theory based on processes in the leading edge of propagating fronts to examine the effect of nonlinearity and weak variation in the background flow. Detailed comparisons are made with numerical experiments for a simple model system.

Key words. atmospheric science, asymptotics

AMS subject classifications. 86A10, 76C15

PII. S0036139900382978

1. Introduction. Observations [6, 13] establish that midlatitude storm tracks live longer and propagate farther and faster than traditional theories would predict. The midlatitude (20–70°) storm track is a disturbance in the atmosphere comprised of a group of eddies which move eastward as a wave packet, gaining energy from strong shears which exist at middle latitudes, and are responsible for much of the weather we experience. A fuller understanding of the mechanisms responsible for the generation of these storms would be very useful for weather prediction, perhaps leading to a significant increase in prediction times.

The storm track consists of a short wave packet containing roughly half a dozen eddies. They are formed at the eastern edges of continents, where diabatic heating leads to increased instability. Maximum "eddy activity" is found downstream, in regions of weaker instability. This wave packet then travels through the region of weaker instability. This is referred to as "downstream development." While the storm track has a life cycle measured in weeks and may circle the entire globe, it is composed of eddies whose individual lifetimes may be only 3–6 days.

The mechanism behind the storm track is the "baroclinic instability." Solar heating causes a strong equator-to-pole temperature gradient. This sets up a density gradient, which competes at midlatitudes with the effect of the earth's rotation and leads to the "thermal wind balance"—a vertical shearing of the predominant westerlies that make up the jet stream. The instability associated with this shear, the baroclinic instability, is responsible for the generation of storms in this region. In the region where storm tracks form, the underlying atmospheric flow is absolutely unstable, which means that localized disturbances may grow *in place* unbounded if the growth is not arrested by nonlinear processes. Downstream, the atmosphere is

convectively unstable, which means that localized growing disturbances eventually move away and disturbances remain bounded at any point in space. These definitions will be made precise in the text.

Several phenomena related to storm track propagation are generally referred to as "downstream development," including the following observations: eddy activity achieves its maximum downstream of the region of absolute instability, and the storm track propagates easily through the downstream region. Storm tracks are observed to move faster than would be predicted by envelope equations based on modulations of unstable normal modes. This is consistent with observations that dynamics at the leading edge have a dominant effect on the growth of the wave packet and that the group velocity of the propagating wave packet exceeds its phase velocity—so that the packet appears to propagate by forming new eddies at its leading edge.

Downstream development has been observed in a number of observational and numerical studies. For the southern hemisphere, Held and Lee [13] study European Center for Medium-Range Weather Forecasting (ECMWF) data and observe clear examples of downstream developing wave packets. These wave packets correspond to storm systems made up of several eddies, which may circle the globe several times. They estimate phase speeds of individual crests and group speeds of entire wave packets. The group velocity is approximately five times the phase velocity, implying downstream development. For the northern hemisphere, Chang [6] makes similar observations also based on ECMWF data. Observing such structures is more difficult in the northern hemisphere, where there are more land-sea interfaces and the storm track is less stable.

In a collection of 1993 papers [5, 6, 18], Chang and Orlanski observe downstream development in numerical experiments for a three-dimensional primitive equation model. This model, together with simpler models they also study, consists of a steady flow containing a vertical shear and usually a jet structure in the meridional direction to model the jet stream. They identify and quantify mechanisms by which energy flows toward the downstream end of the wave packet causing new eddies to develop. They compute an energy budget and find the relative strengths of the various energy fluxes at different points of the wave packet. At the leading edge, the energy transfers are dominated by an "ageostrophic flux" term. This energy flux is due to *linear* terms in the perturbation equations which describe the evolution of the storm track when the average state of the system is imposed externally. They also note that in numerical experiments, waves which are seeded in a region of absolute instability are able to propagate easily through a region of convective instability, and that the only constraint on the distance of propagation is the size of the channel they study.

Held and Lee [13] study a series of models of increasing simplicity: an idealized global circulation model, a two layer primitive equation model, and a two layer system of coupled quasi-geostrophic equations. In all cases they see the signs of downstream development. Significantly, they find that their simplest model, the two layer quasi-geostrophic channel with the earth's rotation and curvature modeled by the β-plane approximation, produces downstream developing wave packets. They show that their wave packets fail to satisfy a typical nonlinear Schrödinger description that might be derived from a normal-mode expansion and suggest that an envelope equation description of their wave packets might be very interesting.

Swanson and Pierrehumbert [23] numerically study a similar two layer quasi-geostrophic system, perturbed about a jet-like shear flow. They initialize a wave packet centered on the linearly most unstable normal mode. Initially, this normal

mode dominates the evolution, but at longer times, leading edge modes dominate the evolution, propagating essentially decoupled from the nonlinear processes at the rear.

We will explore the interaction between the leading edges of storm tracks and a slowly varying shear flow. Some other studies of the baroclinic instability in a variable environment have focused on local and global modes for baroclinically unstable media (Merkine and Shafranek [16]). These are basically eigenmode analyses which apply a linear theory throughout the domain. As the studies by Held and Lee [13] and Swanson and Pierrehumbert [23] show that linear theory is dominant only at the leading edge, we do not follow the global mode approach.

We derive an envelope approximation of the type suggested by Held and Lee but centered on waves with complex wavenumber which dominate the linear leading edge behavior. Others have constructed such a theory for unstable normal modes, such as Pedlosky [19] and, more recently, Esler [9]. The physical relevance of such a construction is questionable because, well behind the front, the solution is large, and thus nonlinear interactions are large as well. The only place where the solution is small enough to apply weakly nonlinear theory is in the leading edge, and thus it is in this restricted domain where an envelope approximation is most likely to apply. Moreover, it is in this very region where the mechanisms of downstream development are active. Thus we design our asymptotic construction for this region. We note that the wavenumbers which are dominant at the leading edge of a wave packet are not necessarily the same as those which dominate the wave packet toward the rear, as seen in the numerical experiments of Swanson and Pierrehumbert [23] as well as in analytic studies, including those of Briggs [2] and Dee and Langer [7].

This study addresses two issues. First, we examine the effects of varying several physical parameters, notably the β-plane effect and the width of the channel in which the wave propagates, on the speed and wavenumber of the leading edge front solutions. We then derive a general set of envelope equations that describe the behavior of the leading edge front solutions to PDEs with slowly variable media, which we use to model the fact that the atmosphere is absolutely unstable where storm tracks develop but convectively unstable downstream. We apply these methods to derive amplitude equations for the leading edge fronts of storm tracks in different physical parameter regimes when the shear flow is allowed to contain spatial variation. We also discuss the effects of varying the parameters on the solutions obtained.

In section 2, we introduce the model equations describing winds at midlatitudes. We discuss mathematical methods used to obtain information about the leading edges of waves in unstable media and apply these methods to our model system, examining the effect of the various physical parameters separately and together. In section 3, we examine the effect of slowly varying media on the leading edges via a multiple scales expansion, which results in modulation equations for the leading edges of storm tracks under varying physical parameters. Finally, in section 4, we perform numerical experiments to verify the validity of the modulation equations on a simpler set of model equations.

2. Linear leading edge theory for baroclinic systems.

2.1. A mathematical model for midlatitude storm tracks.
We begin with the simplest physical model shown by Held and Lee [13] to capture the phenomenon of downstream development. Although the Charney model is the considered the least complex system to accurately capture the full dispersion dynamics of the midlatitude baroclinic instability [10], we choose to work with a simpler two layer model in order to further develop the theory to handle weak variations in the medium in section 3.

We consider a fluid idealized to two shallow immiscible layers of slightly different densities, bounded above by a rigid lid at height D. The system is in a rapidly rotating reference frame with a variable rate of rotation given by

$$\Omega = \frac{1}{2}(f_0 + \beta' y'),$$

where y' is the (dimensional) distance in the meridional direction, to model the curvature of the earth. (This linear variation of the rotation rate along the meridional direction is derived as a first order approximation to the local normal component of the earth's rotation in a small band centered at middle latitude.) We include a drag term to model dissipation at the earth's surface proportional to r' times the lower layer velocity. We choose the physical scales $[L, D, L/U, U, DU/L]$ for the horizontal coordinates, the vertical coordinate, time, and horizontal and vertical velocities. Then, assuming the *Rossby number* $Ro = U/f_0 L$ to be small, which indicates a balance between gravitation and the effects the earth's rotation, we have the standard quasi-geostrophic potential vorticity equations:

$$
\begin{aligned}
(1) \quad & \left(\frac{\partial}{\partial t} + \frac{\partial \Psi_1}{\partial x}\frac{\partial}{\partial y} - \frac{\partial \Psi_1}{\partial y}\frac{\partial}{\partial x}\right)(\Delta \Psi_1 + F(\Psi_2 - \Psi_1) + \beta y) = 0, \\
& \left(\frac{\partial}{\partial t} + \frac{\partial \Psi_2}{\partial x}\frac{\partial}{\partial y} - \frac{\partial \Psi_2}{\partial y}\frac{\partial}{\partial x}\right)(\Delta \Psi_2 + F(\Psi_1 - \Psi_2) + \beta y) + r\Delta \Psi_2 = 0.
\end{aligned}
$$

The nondimensional parameters which appear are

$$\beta = \beta' L^2/U,$$
$$F = \frac{2\rho_2 f_0^2 L^2}{gD(\rho_1 - \rho_2)},$$
$$r = r' L/U.$$

The functions Ψ_1 and Ψ_2 are the upper and lower layer stream functions, so the velocity in each layer is given by

$$\mathbf{u}_j = \left(-\frac{\partial \Psi_j}{\partial y}, \frac{\partial \Psi_j}{\partial x}\right).$$

For constant $u_j = U_j$, one has the exact solution

$$\Psi_i = -U_i y, \quad i = 1, 2,$$

a constant zonal flow in each layer. A full derivation of these equations is given in [20].

We will be concerned with this system in two idealized geometries: in the first, the domain is unbounded in both dimensions. In the second, the fluid is confined to a channel of finite width in the meridional (y) direction and of infinite extent in the zonal (x) direction. In this second case we have the boundary conditions

$$\left.\frac{\partial \Psi_j}{\partial x}\right|_{y=y_{\min}, y_{\max}} = 0.$$

We write perturbation equations by letting

$$\Psi_i = -U_i y + \psi_i, \quad i = 1, 2,$$

and by letting

$$\text{(2)} \qquad U_T = \frac{U_1 + U_2}{2}, \qquad U_B = \frac{U_1 - U_2}{2}$$

be the barotropic and baroclinic parts of the background flow, respectively. The perturbation equations are

$$\text{(3a)} \quad \left(\frac{\partial}{\partial t} + U_1 \frac{\partial}{\partial x} + \frac{\partial \psi_1}{\partial x} \frac{\partial}{\partial y} - \frac{\partial \psi_1}{\partial y} \frac{\partial}{\partial x} \right)$$
$$\left(\Delta \psi_1 + F(\psi_2 - \psi_1) + (\beta + 2FU_B) \frac{\partial \psi_1}{\partial x} \right) = 0,$$

$$\text{(3b)} \quad \left(\frac{\partial}{\partial t} + U_2 \frac{\partial}{\partial x} + \frac{\partial \psi_2}{\partial x} \frac{\partial}{\partial y} - \frac{\partial \psi_2}{\partial y} \frac{\partial}{\partial x} \right)$$
$$\left(\Delta \psi_2 + F(\psi_1 - \psi_2) + (\beta - 2FU_B) \frac{\partial \psi_2}{\partial x} \right) + r\Delta \psi_2 = 0.$$

Equations (3) are in dimensional variables with all parameters explicitly represented in the equations. We begin by rescaling the equations to reduce the number of parameters. We make the scalings

$$\text{(4)} \quad \left[\tilde{x} = \sqrt{F}x; \tilde{y} = \sqrt{F}y; \tilde{t} = \sqrt{F}U_B t; \tilde{\psi}_i = \frac{U_B \psi_i}{\sqrt{F}}; \tilde{U}_i = \frac{U_i}{U_B}; \tilde{\beta} = \frac{\beta}{U_B F}; \tilde{r} = \frac{r}{U_B F} \right]$$

and change variables to the moving reference frame

$$\tilde{x} \to \tilde{x} - \tilde{U}_T t,$$

which makes the mean velocities in each layer $\tilde{U}_1 = 1$ and $\tilde{U}_2 = -1$ and allows us to work with a system in only three parameters: β, r, and the nondimensional channel width. (Note that working in a reference frame moving at the mean velocity $\tilde{U}_T$ is equivalent to working in a system with zero mean flow.)

We drop the tildes and obtain the dimensionless equations, dependent only on the parameters β and r.

$$\text{(5a)} \quad \left(\frac{\partial}{\partial t} + \frac{\partial}{\partial x} + \frac{\partial \psi_1}{\partial x} \frac{\partial}{\partial y} - \frac{\partial \psi_1}{\partial y} \frac{\partial}{\partial x} \right) (\Delta \psi_1 + (\psi_2 - \psi_1)) + (\beta + 2) \frac{\partial \psi_1}{\partial x} = 0,$$

$$\text{(5b)} \quad \left(\frac{\partial}{\partial t} - \frac{\partial}{\partial x} + \frac{\partial \psi_2}{\partial x} \frac{\partial}{\partial y} - \frac{\partial \psi_2}{\partial y} \frac{\partial}{\partial x} \right)$$
$$(\Delta \psi_2 + (\psi_1 - \psi_2)) + (\beta - 2) \frac{\partial \psi_2}{\partial x} + r\Delta \psi_2 = 0.$$

We may write this system as a general differential equation consisting of a linear and a quadratic part:

$$\text{(6)} \quad \mathcal{L} \left(-i\frac{\partial}{\partial x}, -i\frac{\partial}{\partial y}, i\frac{\partial}{\partial t} \right) \begin{pmatrix} u_1(x,t) \\ u_2(x,t) \end{pmatrix} + \mathcal{B} \left(-i\frac{\partial}{\partial x}, -i\frac{\partial}{\partial y}, i\frac{\partial}{\partial t} \right) (\vec{u}, \vec{u}) = 0,$$

where in (5)

$$\vec{u} = \vec{\psi},$$

$$\mathcal{L} = \begin{bmatrix} (\partial_t + \partial_x)(\Delta - 1 + (\beta + 2)\partial_x) & \partial_t + \partial_x \\ \partial_t - \partial_x & (\partial_t - \partial_x)(\Delta - 1 + (\beta - 2)\partial_x) + r\Delta \end{bmatrix},$$

$$\mathcal{B}(\vec{\psi}, \vec{\psi}) = \begin{bmatrix} (\partial_x \psi_1 \partial_y - \partial_y \psi_1 \partial_x)(\Delta\psi_1 + (\psi_2 - \psi_1) + (\beta + 2)\partial_x\psi_1) \\ (\partial_x \psi_2 \partial_y - \partial_y \psi_2 \partial_x)(\Delta\psi_2 + (\psi_1 - \psi_2) + (\beta - 2)\partial_x\psi_2) \end{bmatrix}.$$

For the asymptotic methods that follow we require that the linearized version of (6) be unstable in the sense we now describe in section 2.2.

2.2. Derivation of marginal stability/leading edge speed. We describe a method for finding leading edge "marginal stability" velocities for linear waves—as put forward by Briggs in [2] and well summarized in Huerre and Monkewitz [14]. This is based on linear processes in the leading edges, noting that Orlanski and Chang [18] found *linear* ageostrophic flux terms to be the dominant mode of energy transfer in simulations of downstream developing baroclinic systems and that Swanson and Pierrehumbert [23] found that propagation is controlled by leading edge dynamics.

Consider a y-independent linearized form of our generalized equation (6):

$$(7) \qquad \mathcal{L}\left(-i\frac{\partial}{\partial x}, i\frac{\partial}{\partial t}\right) \begin{pmatrix} u_1(x,t) \\ u_2(x,t) \end{pmatrix} = 0,$$

where $\mathcal{L}$ is a matrix valued polynomial in two variables. This has solutions of the form

$$(8) \qquad \begin{pmatrix} u_1(x,t) \\ u_2(x,t) \end{pmatrix} = \begin{pmatrix} 1 \\ \gamma(k,\omega) \end{pmatrix} e^{i(kx-\omega t)}$$

for ω and k satisfying the dispersion relation

$$(9) \qquad \Delta(k,\omega) = \det \mathcal{L}(k,\omega) = 0.$$

The general solution to (7) is given by a space-time convolution with Green's function, which satisfies

$$(10) \qquad \mathcal{L}\left(-i\frac{\partial}{\partial x}, i\frac{\partial}{\partial t}\right) G(x,t) = \begin{bmatrix} \delta(x)\delta(t) & 0 \\ 0 & \delta(x)\delta(t) \end{bmatrix}.$$

$G(x,t)$ may be represented by a Fourier–Laplace integral,

$$(11) \qquad G(x,t) = \frac{1}{4\pi^2} \int_\Gamma d\omega \int_{-\infty}^{\infty} dk \frac{e^{i(kx-\omega t)}}{\Delta(k,\omega)} \begin{bmatrix} \mathcal{L}_{2,2} & -\mathcal{L}_{1,2} \\ -\mathcal{L}_{2,1} & \mathcal{L}_{1,1} \end{bmatrix},$$

where Γ, the *Bromwich contour*, is a horizontal line in the complex plane lying above $\operatorname{Im}\omega = \sigma$, $\mathcal{L}_{i,j}$ are the entries of the matrix $\mathcal{L}$, and

$$\sigma = \max_{k \in \mathbb{R}} \omega(k).$$

This choice of Γ ensures causality by allowing the ω-integral to be closed in the upper half plane for $t > 0$. The leading term of the asymptotics for $t \gg 1$ will be given by

$$(12) \qquad G(x_0, t) \approx \frac{i e^{i(k^* x_0 - \operatorname{Re}(\omega^* - v^* k^*)t \pm \frac{\pi}{4})}}{t^{\frac{1}{2}} \sqrt{2\pi \left(\frac{\partial\Delta}{\partial\omega}\frac{\partial^2\Delta}{\partial k^2}\right)_{k^*,\omega^*}}} \begin{bmatrix} \mathcal{L}_{2,2}(k^*,\omega^*) & -\mathcal{L}_{1,2}(k^*,\omega^*) \\ -\mathcal{L}_{2,1}(k^*,\omega^*) & \mathcal{L}_{1,1}(k^*,\omega^*) \end{bmatrix},$$

where the quantities k^*, ω^*, and v^* are defined in the discussion below.

We will study the asymptotic behavior of solutions as $t \to \infty$ along the ray $x = x_0 + vt$. We will first show how to find the "local growth rate" in the reference frame $v = 0$ and then show how to extend this argument to a moving reference frame with velocity $v \neq 0$. We fix $x = x_0$ and study the behavior of solutions as $t \to \infty$. First, we evaluate the k-integral. For $x_0 > 0$ the Fourier contour must be closed in the upper half k-plane. For each ω on the Bromwich contour, we define the pole loci as

$$PL(\omega) = \{k_n | \Delta(k_n, \omega)\} = 0.$$

The pole loci then determine the singularities of the integral (11). If $\Delta(\omega, k)$ is Nth degree in k, then for each ω on the Bromwich contour, the pole loci contain N roots, the first N^+ of which lie in the upper half plane. The k-integral in (11) can then be evaluated by residues,

$$(13) \qquad G(x_0, t) = \frac{i}{\pi} \int_\Gamma \sum_{n=1}^{N^+} \frac{e^{i(k_n x_0 - \omega t)}}{\frac{\partial \Delta(k_n, \omega)}{\partial k}} \begin{bmatrix} \mathcal{L}_{2,2}(k_n, \omega) & -\mathcal{L}_{1,2}(k_n, \omega) \\ -\mathcal{L}_{2,1}(k_n, \omega) & \mathcal{L}_{1,1}(k_n, \omega) \end{bmatrix} d\omega.$$

To evaluate the remaining integral for large t, the Bromwich contour Γ should be deformed downward as far as possible in the complex ω-plane. The asymptotics are then dominated by the singularity in the ω-plane with the largest imaginary part. Note, however, that the pole loci are defined in terms of the ω-contour, and shifting Γ also causes the pole loci to shift. When Γ lies entirely above the line $\text{Im}\,\omega = \sigma$, then the pole loci do not intersect the real k-axis, as σ is the maximum imaginary part of ω for any k on the real axis. As Γ is shifted downward below this line, however, the pole loci may intersect the real k-axis on which the Fourier integral is performed. Thus, as Γ is deformed, the k integration contour must be deformed to avoid the singularities of this integral. As the k-contour is deformed, the pole loci also deform. For critical values of ω, two branches of the pole loci may coalesce. This deformation process is shown in Figure 2.1.

When two poles on the pole loci coalesce, one of two things may happen. If two pole loci from the same side of the k-contour coalesce, they will not contribute to the integral, as two coalescing first order poles form a pure second order pole, which has zero residue. If two poles from loci on opposite sides of the k-contour coalesce, then the k-contour is "pinched" between the pole loci, and Γ can not be lowered any further. Let ω_s be the uppermost point in the ω-plane for which two pole loci cross from opposite sides of the Fourier contour, and let k_s be the point in the k-plane where they cross. Clearly, where two pole loci coalesce the dispersion relation (9) must have a double root so that

$$(14) \qquad \frac{\partial \Delta}{\partial k}(k_s, \omega_s) = 0.$$

Thus finding a saddle point of $\Delta(k, \omega)$ is a necessary condition for finding the dominant term in the asymptotics but not a sufficient one, as the double root must arise from a "pinching" of the Fourier contour between the pole loci.

Note that as $(k, \omega) \to (k_s, \omega_s)$, the denominator in (13) goes to zero so that the integral is singular at this point. To evaluate this integral asymptotically, we expand
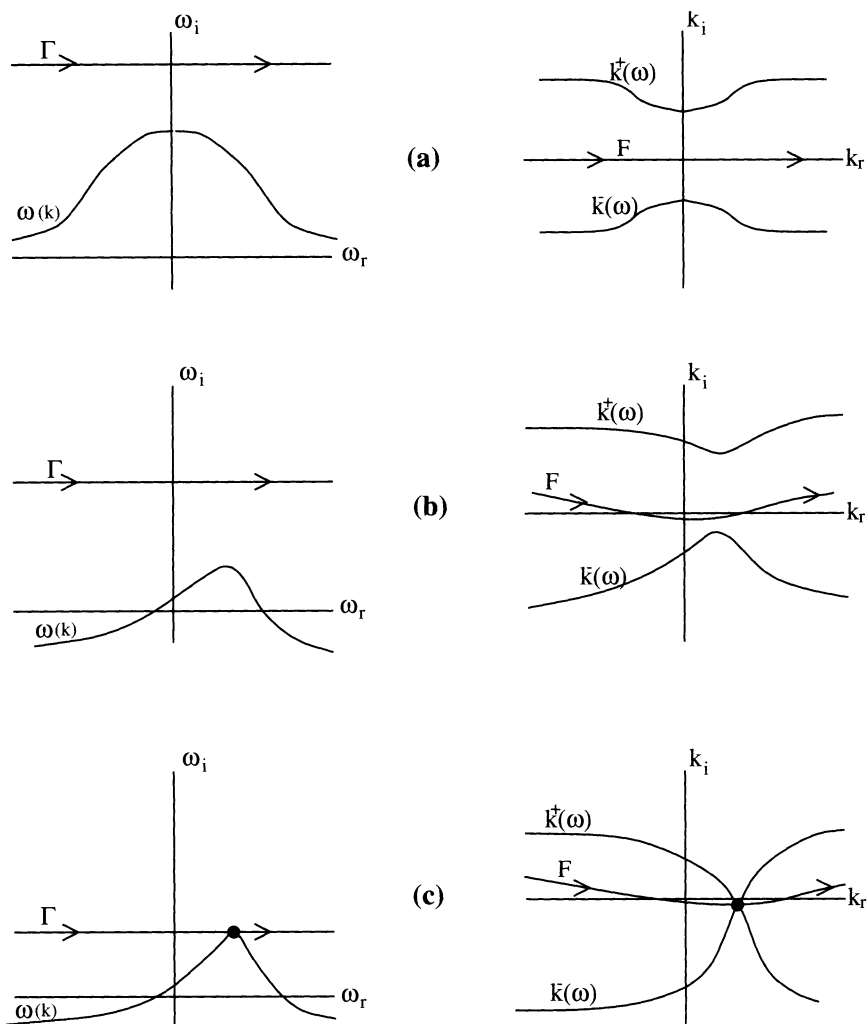
FIG. 2.1. *To asymptotically evaluate the double integral over the Bromwich contour Γ and the Fourier contour F in* (a), *the contour Γ is shifted downward,* (b), *which requires a shift of F, until a singularity is met,* (c), *and F becomes "pinched" between the images of Γ in the k-plane. This figure is reproduced from* [14].

it in the neighborhood of the singularity (14). Repeated use of Taylor's theorem yields

$$\frac{\partial \Delta}{\partial k} \approx \pm \sqrt{-2(\omega - \omega_s)\left(\frac{\partial \Delta}{\partial \omega}\frac{\partial^2 \Delta}{\partial k^2}\right)_{k_s,\omega_s}},$$

the sign of which will depend on the specific problem. The denominator in (13) thus vanishes as $(\omega - \omega_s)^{\frac{1}{2}}$, and the leading term of the integral in (13) may be obtained from the expansion about this singularity:

$$(15) \qquad G(x_0, t) \approx \frac{ie^{i(k_s x_0 - \omega_s t \pm \frac{\pi}{4})}}{t^{\frac{1}{2}}\sqrt{2\pi\left(\frac{\partial \Delta}{\partial \omega}\frac{\partial^2 \Delta}{\partial k^2}\right)_{k_s,\omega_s}}}\begin{bmatrix} \mathcal{L}_{2,2}(k_s,\omega_s) & -\mathcal{L}_{1,2}(k_s,\omega_s) \\ -\mathcal{L}_{2,1}(k_s,\omega_s) & \mathcal{L}_{1,1}(k_s,\omega_s) \end{bmatrix}.$$

The exponential growth rate in the stationary frame is thus given by $e^{\text{Im}\,\omega_s}$. We may extend this analysis to find the growth rate in a reference frame moving at constant velocity v by considering the behavior as $t \to \infty$ with $x = x_0 + vt$. This is equivalent to a change of variables to $(\tilde{x} = x - vt,\ \tilde{t} = t)$. We repeat the preceding analysis in this frame with $\tilde{\omega} = \omega - vk$ and $\tilde{k} = k$. The growth rate in the reference frame moving at constant velocity v is thus given by $e^{\text{Im}\,\tilde{\omega}_s} = e^{\text{Im}(\omega_s - vk_s)}$. The dispersion relation is independent of the moving reference frame, while the saddle point condition can be written in the original variables, (k, ω), as

$$(16) \qquad \frac{\partial \Delta}{\partial k}(k_s, \omega_s) - v\frac{\partial \Delta}{\partial \omega}(k_s, \omega_s) = 0.$$

Suppose that there exists a finite range of velocities (v_t, v_l) such that the growth rate $\text{Im}\,\tilde{\omega}_s(v)$ is positive for reference frame velocities in this interval and vanishes at the endpoints v_t and v_l. These velocities define a wave packet which is both expanding in space and growing in amplitude. The *trailing edge speed* will be given by v_t, and the *leading edge speed* will be given by v_l. These are referred to as *marginal stability* velocities because they mark the transition between reference frames in which the solution is growing to those in which it is decaying. We will denote the leading edge marginal velocity by v^* and the associated wavenumber and frequency in that reference frame k^* and ω^*. The marginality condition can be written as

$$(17) \qquad \text{Im}\,\tilde{\omega}^* = \text{Im}\,(\omega^* - v^*k^*) = 0.$$

An unstable system is deemed *absolutely unstable* if $0 \in (v_t, v_l)$, that is, if the growth rate in the stationary frame of reference is positive. In this case a localized disturbance will eventually grow to overtake the entire domain. By contrast, it is *convectively unstable* if $v = 0$ is not contained in the region of instability. In this case, a growing disturbance will eventually move out of any compact region, and the limiting solution is finite at every point in space. We will use the methods described here to discuss the absolute and convective stability properties of the background shear flow at midlatitude.

To summarize, the asymptotic properties of the leading edge wave will be described by the triplet (v^*, k^*, ω^*), which satisfies

$$(18) \qquad \Delta(\omega^*, k^*) = 0, \qquad\qquad \text{the dispersion relation,}$$

$$(19) \qquad \left(\frac{d\Delta}{dk} + v^*\frac{d\Delta}{d\omega}\right)_{k^*, \omega^*} = 0, \qquad\qquad \text{the saddle point condition,}$$

$$(20) \qquad \text{Im}(\omega^* - v^*k^*) = 0, \qquad\qquad \text{the marginality condition,}$$

in addition to the more stringent conditions that the saddle point arise as a true "pinch point" and that this be the largest v^* for which such a triplet exists.

2.3. Numerical implementation of this method. For a complicated system of PDEs, the three preceding conditions will not be solvable in analytic closed form, so a numerical scheme must be implemented to find the leading edge speed. We accomplish this in two steps. First, with v as a parameter, we find all ordered pairs (k, ω) which satisfy the dispersion relation and saddle point condition, (18) and (19), and we determine which of these represent "pinch points" and thus contribute to Green's function. The second step determines the growth rates associated with these wavenumbers and looks for the edges of the stability regions in "velocity space" to determine the leading edge speed.

Our first step is to find all the saddle points of the system. We may eliminate the ω from the pair of equations by forming the resultant of the two polynomials, (18) and (19), when considered as functions of ω [3]. This forms a higher order polynomial in k alone. This is advantageous for two reasons. First, we may simply read from the degree of this polynomial how many common roots are shared by (18) and (19). Second, we may use iterative eigenvalue methods to find the roots of a single polynomial. This method was found to be much more stable and reliable than using a Newton method to jointly solve the system of two polynomials.

To find the leading edge properties of the wave, first the resultant is found symbolically using Maple. Then all the roots k of the resultant are found numerically as a function of the reference frame velocity v. For each of these k, the accompanying frequency ω and growth rate $\mathrm{Im}(\omega - vk)$ are formed. Each root k which gives a positive growth rate is then examined to see if it corresponds to a "pinch point" and contributes to the asymptotic solution. Note that a double root is a pinch point if the two pole loci which join to form the double root are on opposite sides of the Fourier contour before the Bromwich contour is lowered. Therefore, we may simply examine where the two roots go if the imaginary part of ω_s is increased to σ, the maximum growth rate for real wavenumbers. If one root moves to the upper half k-plane and the other root moves to the lower half, then the double root corresponds to a pinch point.

We then examine the growth rates $\mathrm{Im}(\omega - vk)$ of all the growing modes as a function of velocity and find a "region of instability" with respect to the reference frame velocity v. The velocity at the right endpoint of the instability region is then taken to be the leading edge marginal stability velocity, v^*.

2.4. Application to downstream development. We now consider the scaled two layer midlatitude quasi-geostrophic equation (5), and we consider leading edge dynamics with or without β-plane and lower layer Ekman drag effects. We will look primarily at flows with no dependence on y, the cross stream direction, and then generalize to flows in channel geometries.

2.4.1. The inviscid f-plane, no channel. We first present the simplest possible variant of the above system by setting the Coriolis parameter, β, and the coefficient of Ekman damping, r, to zero and assuming a y-independent geometry. We will be able to gain a complete understanding of this system and then may consider the fuller versions perturbatively. We also discover some bifurcations as the parameters are varied, which demonstrates the limitations of the perturbative approach.

We linearize the scaled perturbation equations (5), with $\beta = 0$ and $r = 0$, yielding

$$
(21) \quad
\begin{aligned}
\left(\frac{\partial}{\partial t} + \frac{\partial}{\partial x}\right)(\Delta\psi_1 + (\psi_2 - \psi_1)) + 2\frac{\partial\psi_1}{\partial x} &= 0, \\
\left(\frac{\partial}{\partial t} - \frac{\partial}{\partial x}\right)(\Delta\psi_2 + (\psi_1 - \psi_2)) - 2\frac{\partial\psi_2}{\partial x} &= 0.
\end{aligned}
$$

If we look for sinusoidal normal-mode solutions of the form (8), then (ω, k) must satisfy the dispersion relation

$$
(22) \qquad \Delta(\omega, k) = k^6 - (\omega^2 + 2)k^4 - 2\omega^2 k^2, \text{ or}
$$

$$
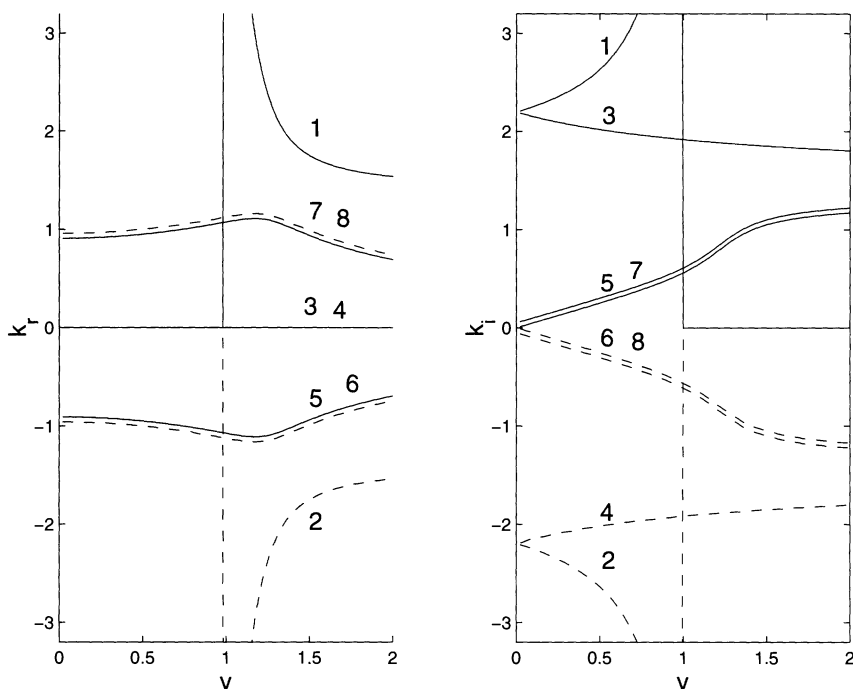\omega = \pm k\sqrt{\frac{k^2 - 2}{k^2 + 2}}.
$$

FIG. 2.2. *The selected wavenumbers as a function of reference frame velocity. There are eight waves selected in each reference frame, labeled* 1–8.

Thus the disturbances of wavenumber $k^2 < 2$ are unstable. The saddle point condition (19) in the reference frame moving at velocity v is given by

$$(23) \qquad 6k^5 - 2\omega k^4 v - (8 + 4\omega^2)k^3 - 4\omega v k^2 - 4\omega^2 k = 0.$$

Eliminating ω between (22) and (23) yields

$$(24) \qquad (1 - v^2)k^8 + (8 - 4v^2)k^6 + 8k^4 + (16v^2 - 32)k^2 + 16 + 16v^2 = 0.$$

Thus, implementing the procedure described in section 2.3, solving this final equation with v as a parameter gives us a set of eight "candidate" wavenumbers. Figure 2.2 shows the selected wavenumbers as a function of the reference frame velocity v. Only those with $\operatorname{Im} k > 0$ are relevant in the leading edge of a disturbance, as the solution must decay as $x \to +\infty$.

Figure 2.3 shows the growth rates for the four right-decaying wave solutions. The two roots labeled 1 and 2 in Figure 2.2 which diverge to ∞ as $v \to 1$ do not satisfy the pinch point condition so do not contribute to the integral.

The point where the last curve crosses the axis is the marginal reference velocity and is marked with a star in Figure 2.3. For this system, the leading edge speed may be found exactly. The critical velocity is $v^* = \sqrt{2}$. At this velocity, the coefficients of k^2 and k^6 in (24) vanish so that (24) becomes

$$k^8 - 8k^4 - 48 = 0,$$

which may be solved by the quadratic formula. The two roots $k_\pm = \pm 1 + i$ represent the exact wavenumbers making up the leading edge of the wave. The leading edge
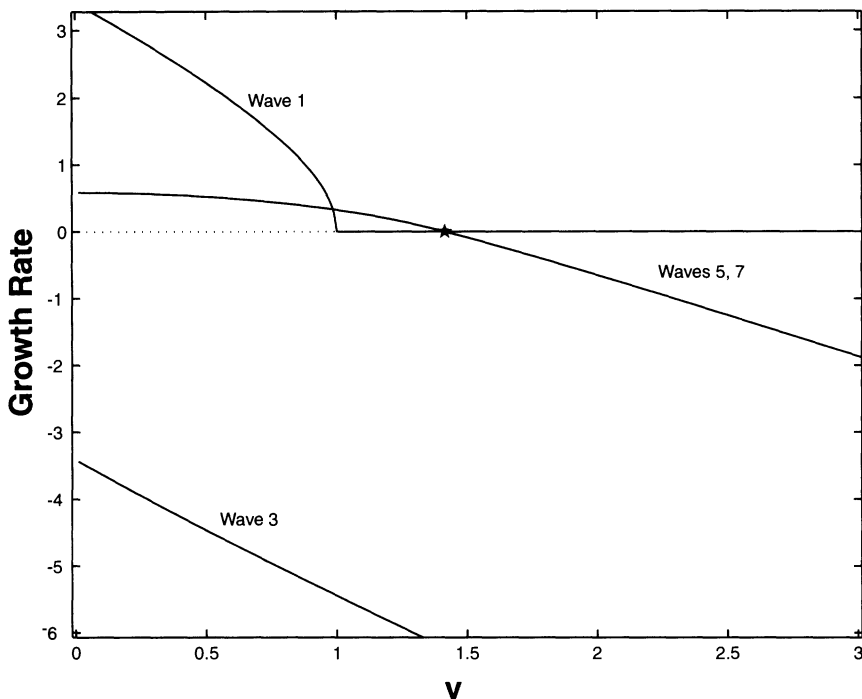
FIG. 2.3. *The growth rate of the waves which are right-decaying as a function of reference frame velocity. A star marks the speed $v = \sqrt{2}$, at which the system is neutrally stable.*

properties are thus given by

$$(25) \qquad \left(k^* = \pm 1 + i; \omega^* = \sqrt{2}i; v^* = \sqrt{2} \right).$$

We may use this analysis to clarify a point made by Merkine in [15]. He finds that $|U_T| < \sqrt{2}\,|U_B|$ is a necessary and sufficient criterion for absolute instability. Recall that we have chosen $U_T = 0$ and $U_B = 1$. If U_T and U_B are chosen generally, then the leading and trailing edge velocities are $v_\pm = U_T \pm \sqrt{2}U_B$. If $v_- = U_T - \sqrt{2} < 0$, then the system is absolutely unstable, which is Merkine's condition.

2.4.2. The addition of the β-plane effect. Next we investigate the effect of reintroducing the β-plane terms into the equations. We linearize the scaled perturbation equations (5), with $\beta > 0$, yielding

$$(26) \qquad \begin{aligned} \left(\frac{\partial}{\partial t} + \frac{\partial}{\partial x} \right) (\Delta \psi_1 + (\psi_2 - \psi_1)) + (\beta + 2)\frac{\partial \psi_1}{\partial x} &= 0, \\ \left(\frac{\partial}{\partial t} - \frac{\partial}{\partial x} \right) (\Delta \psi_2 + (\psi_1 - \psi_2)) + (\beta - 2)\frac{\partial \psi_2}{\partial x} &= 0. \end{aligned}$$

Again, we substitute the ansatz (8) and find the dispersion relation

$$(27) \qquad \Delta(k, \omega) = k^6 - (\omega^2 + 2)k^4 - 2\beta\omega k^3 - (2\omega^2 + \beta^2)k^2 - 2\omega k\beta = 0.$$

We may solve the dispersion relation for ω with real k,

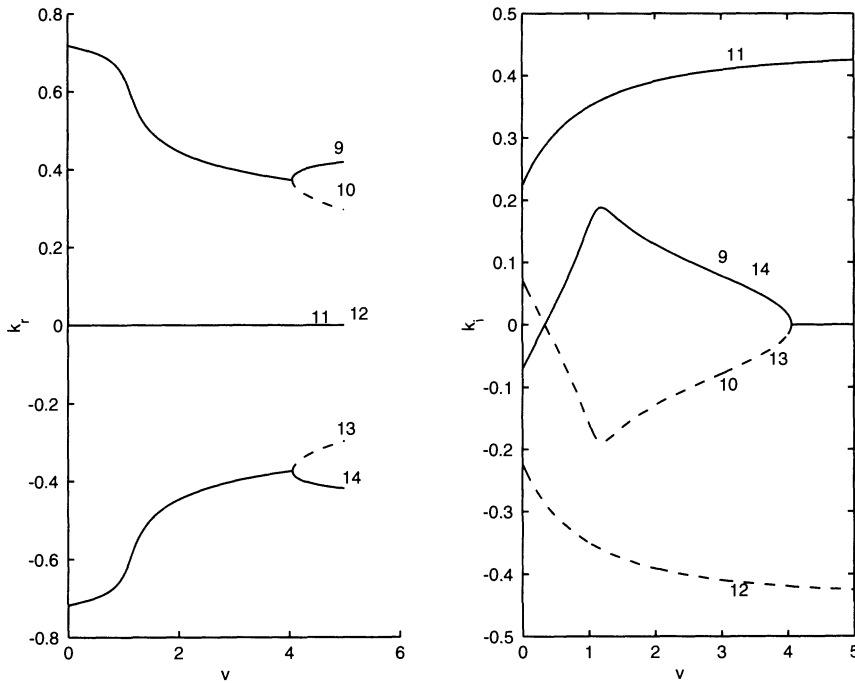$$\omega = \frac{-\left(k^2 + 1\right)\beta \pm \sqrt{\beta^2 + k^8 - 4k^4}}{k\left(k^2 + 2\right)},$$

FIG. 2.4. *The wavenumbers representing the six roots of the β-plane resultant which are not present in the f-plane model. Solid lines denote positive imaginary parts; dashed curves denote negative imaginary parts.*

and find that this may give growing normal modes if $\beta < 2$. (It is more standard to write the condition for instability in terms of a critical shear U_B [19], which we have scaled to equal one.) The f-plane system is unstable for any velocity, so the β-plane effect stabilizes the background shear flow.

We find that k now satisfies a polynomial of degree 14, yielding 14 possible values of k for each v. For the f-plane equations, there were only 8 roots, so 6 new roots arise when β is increased from zero. The six "new" waves are shown in Figure 2.4 for the case $\beta = 0.1$. The structure remains very similar as β is increased. Our initial expectation was that the leading edge speed for small β would be a small perturbation of the leading edge speed for of the f-plane equations. The new roots instead change the behavior dramatically.

For small values of β, the new roots and the old roots seem to behave independently of each other. The roots relevant to the leading edges are labeled 9 and 14 in Figure 2.4. These are not simply perturbations of the roots which give the leading edge for the f-plane equations. They display an interesting and unexpected behavior. At a specific value of v, to the right of the marginal point for the f-plane equations, two pairs of conjugate roots coalesce at a finite v_{critical} and for $v > v_{\text{critical}}$ have zero imaginary part. This bifurcation point, which corresponds to the largest marginal stability velocity, is clearly visible in Figure 2.4. The Briggs procedure fails, as the leading wave behavior is given by a nongeneric higher order saddle point, corresponding to a quadruple root of the dispersion relation (27). Therefore, $\bar{\omega}''(k^*) = 0$, Briggs's asymptotic formula (12), does not directly apply.

As $\beta \to 0$, the resultant factors into the degree 8 f-plane resultant and a second

polynomial of degree 6. From this second polynomial, we may find a perturbative value of the leading edge wavenumber and find that the associated leading edge velocity approaches $v = \sqrt{9 + 6\sqrt{3}}$, which is very close to the numerically obtained values for finite β and nearly three times the speed predicted for the f-plane. This contrasts sharply with the results of studies that include realistic vertical structure, for which the nonzero β causes a net *decrease* in the leading edge speed [22].

2.4.3. The addition of dissipation. Next we reintroduce dissipation in the form of lower layer Ekman damping, which will remove the degeneracy discussed in the previous section. The PDE is given by

$$
\begin{aligned}
\left(\frac{\partial}{\partial t} + \frac{\partial}{\partial x} \right) (\Delta \psi_1 + (\psi_2 - \psi_1)) + (\beta + 2)\frac{\partial \psi_1}{\partial x} = 0, \\
\left(\frac{\partial}{\partial t} - \frac{\partial}{\partial x} \right) (\Delta \psi_2 + (\psi_1 - \psi_2)) + (\beta - 2)\frac{\partial \psi_2}{\partial x} + r\Delta \psi_2 = 0.
\end{aligned}
$$

(28)

The dispersion relation becomes complex, and the resultant equation in k alone is a complex coefficient fourteenth degree polynomial, and the roots no longer occur in conjugate pairs. Dissipation has the expected result of breaking the degeneracy of the leading edge mode and slowing down the leading edge speed slightly. Recall that for the conservative equation, a pair of conjugate roots bifurcates to a pair of real roots at the leading edge speed v^*. Figure 2.5 shows that when dissipation is added, the bifurcation no longer takes place. The structure of the bifurcation remains visible in the perturbed system. The selected wavenumber, however, has an imaginary part of about 10^{-2} so that the basic shape of the leading wave remains sinusoidal when dissipation is added, with only a very slow exponential decay. Figure 2.6 shows the stabilization and the decrease in the speed of the leading edge resulting from the dissipation. It also shows that the growth rate levels off after crossing the marginality point, and does not continue to decay quickly, as was the case for the f-plane leading edge. A more "robust" modification to the leading edge properties will be given by the addition of a channel geometry. For later reference, we present a table of the values at the leading edge with $\beta = 1.6$, the value used by DelSole [8] under our nondimensionalization, and r variable:

(29)

r	v^*	k^*		ω^*	
0	3.45	.835		-1.62	
.05	3.06	.867	$+.099i$	-1.51	$+.30i$
.10	2.86	.887	$+.129i$	-1.44	$+.37i$
.15	2.72	.903	$+.150i$	-1.39	$+.41i$

2.4.4. The effect of the channel geometry. The discussions above have all focused on y-independent geometries, which we will use to examine how y-independent fronts are modulated in the presence of slowly varying media. Many other instability studies [8, 9, 15, 19] focus on channel geometries, where the fluid is bounded between hard walls at $y = 0$ and $y = L$. We examine the effect of the channel width both on the leading edge of the f-plane equations and the more interesting changes that take place in the high order multiple root which characterizes the leading edge for the β equations.

2.4.5. The f-plane equations. The normal-mode solutions to the linearized equations are

$$
\begin{pmatrix} \psi_1 \\ \psi_2 \end{pmatrix} = \begin{pmatrix} 1 \\ \gamma \end{pmatrix} e^{i(kx - \omega t)} \sin ly,
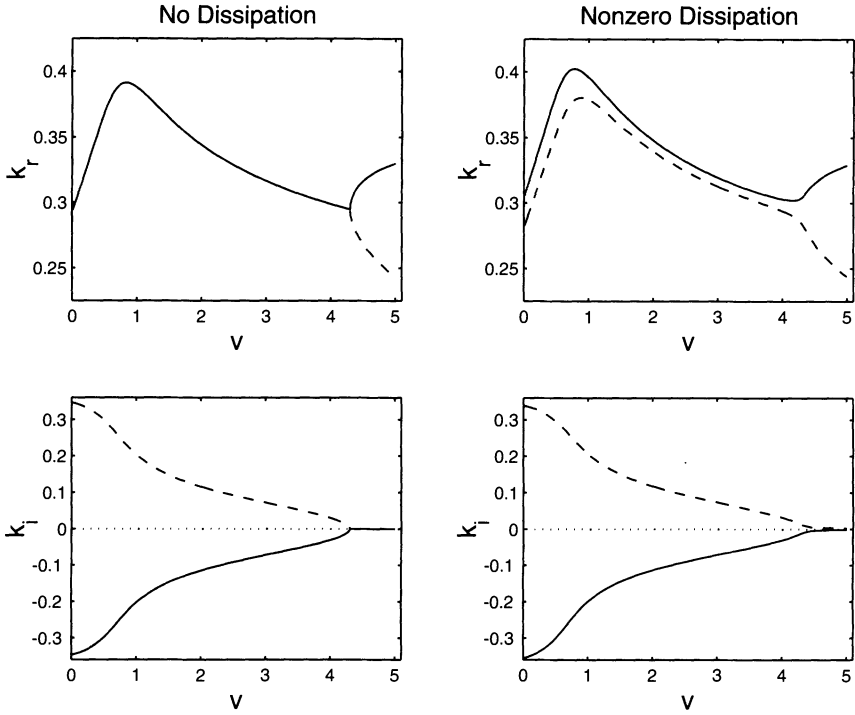$$

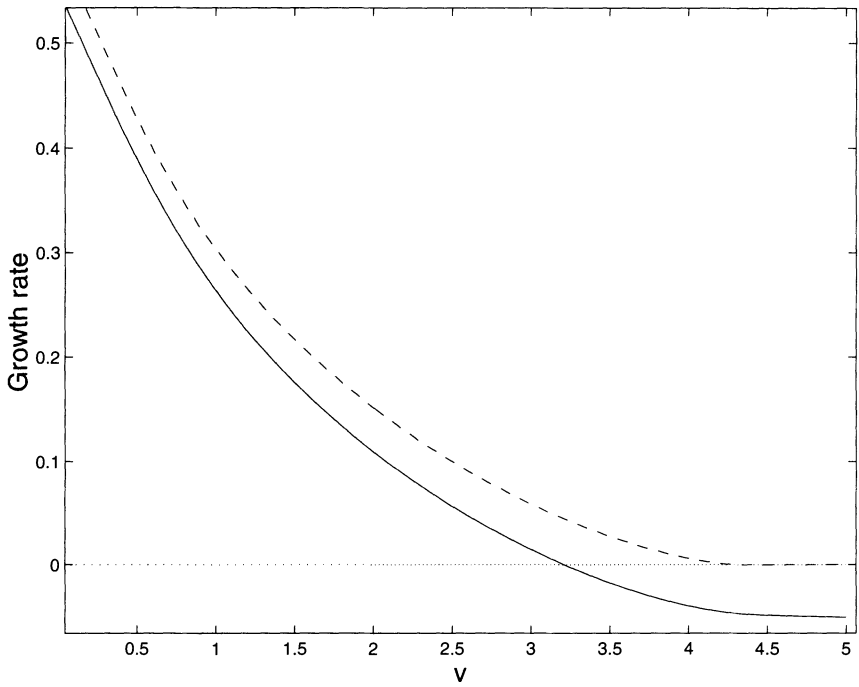FIG. 2.5. *The "breaking" of the bifurcation for the leading edge wave.*

FIG. 2.6. *The growth rate versus velocity for the dissipative (solid line) and zero dissipation (dashed line).*
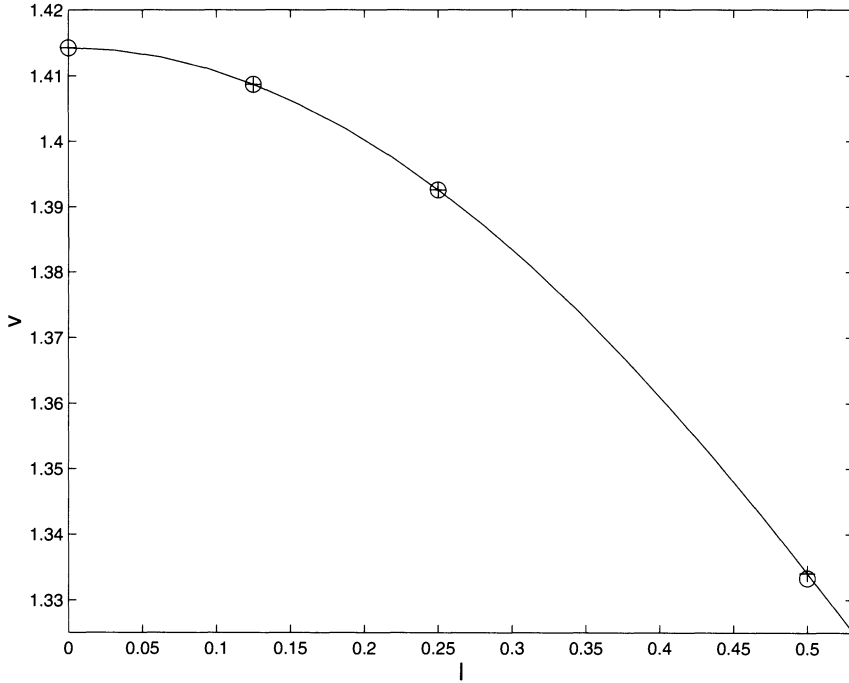
FIG. 2.7. *Marginal stability velocity vs. y-wavenumber l, showing good agreement between the values computed via the perturbation expansion* (+) *and via the numerical procedure* (○).

where $l = \frac{N\pi}{L}$. We shall take $N = 1$ as this mode is the most unstable. The dispersion relation is

$$\Delta(\omega, k) = k^6 + (2l^2 - \omega^2 - 2)k^4 + (-2l^2 - 2\omega^2 - 2l^2\omega^2 + l^4)k^2 - l^4\omega^2 - 2l^2\omega^2.$$

As before, the formula for selected wavenumbers is of fourth degree in k^2.

A wide channel gives rise to a small wavenumber, $l = \epsilon$, which admits the perturbation expansion:

$$(30) \qquad\qquad v^* = \sqrt{2} - \frac{\sqrt{2}}{4}\epsilon^2 + O(\epsilon^4);$$

$$(31) \qquad\qquad k^* = 1 + i + \frac{1}{2}\epsilon^2 + \left(\frac{1}{8} - \frac{i}{4}\right)\epsilon^4 + O(\epsilon^6);$$

$$(32) \qquad\qquad \omega^* = \sqrt{2}i - \epsilon^2\left(\frac{1}{4} + \frac{i}{2}\right) + O(\epsilon^4).$$

The perturbation series gives excellent approximations to the values of the leading edge velocity as shown in Figure 2.7. Merkine [15] finds by a formal argument that the condition for absolute instability of this system is given by $U_B > \sqrt{2}(1 - \frac{l^2}{2})^{1/2}$, which agrees with the perturbation series to leading order.

2.4.6. The β-plane equations in a channel. In this section, we investigate the effect of the channel geometry on the high order root which determines the leading edge wave for the β-plane system. The effect is more dramatic than of simply adding
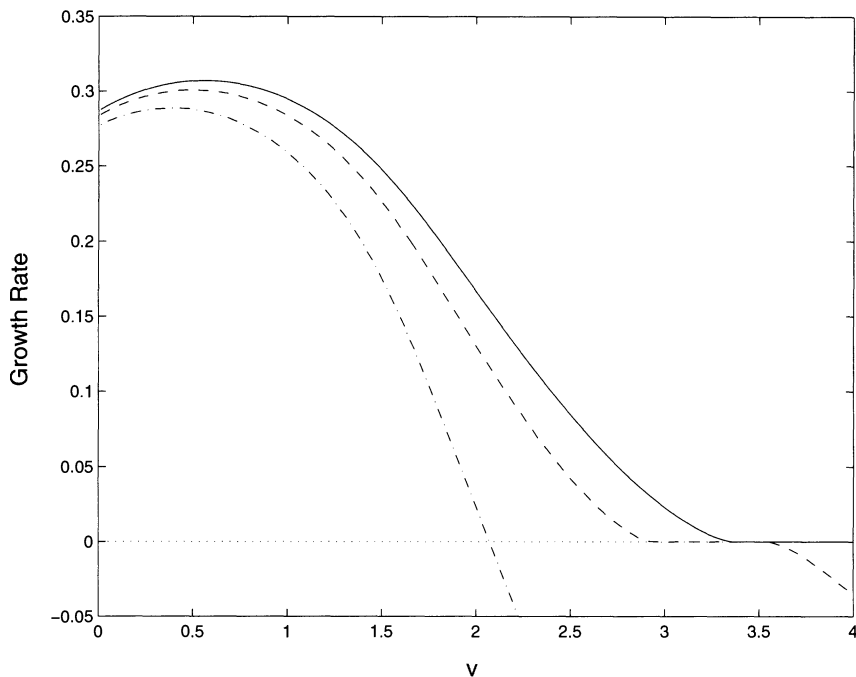
FIG. 2.8. *Growth rate versus velocity with $l = .1$ (solid), $l = .25$ (dashed), and $l = .4$ (dash-dot).*

dissipation. DelSole in [8] studies the β-plane equations in a channel and does not show a high order root at the leading edge. This leads us to study whether the channel geometry is sufficient to remove the degeneracy.

We study the β-plane equations with $r = 0$ and find that k satisfies a polynomial equation of degree 16. We fix $\beta = 1.6$, corresponding to the value used in [8], and decrease the channel width from ∞, which is equivalent to increasing l from zero. The system goes through three stages. (i) When the channel is very wide, the behavior is essentially the same as for a channel of infinite width. (ii) As the channel is narrowed, however, a second high order root forms at a velocity greater than v^*. The two quadruple roots move together as the channel is narrowed further and at some critical channel width annihilate each other. (iii) Beyond this value, the multiple roots disappear, and the system contains no degeneracy. In Figure 2.8, the growth rate is shown as a function of velocity for values of l in the three above regimes. (i) When l is small, the behavior is the same as when $l = 0$. The leading edge wave bifurcates at some finite value of v, beyond which there is no pinch point. (ii) For intermediate l, there exist two critical velocities, separating two unstable wave packets. (iii) For l sufficiently large, these two critical velocities, and hence the associated wave packets, merge, and the leading edge wave is determined by a double root as in the standard Briggs procedure. Such an l corresponds to a channel whose width is two to three times the wavelength in the zonal direction.

This shows that the multiple root which appeared to determine the leading edge behavior is an artifact of the one-dimensional geometry. However, even without this degeneracy, the leading edge speed is significantly enhanced in the presence of nonzero β.

3. Modulation by nonlinearity and weakly variable media. With the description of the marginally stable linear wave front in hand, we now examine the effects that nonlinearity and weak variation in the background shear flow have on downstream developing dynamics. Recall that the atmosphere is absolutely unstable off the eastern shores of continents and convectively unstable over the oceans. An easy way to model this is to allow the strength of the shear to vary slowly. To create a variable medium, we linearize (1) about the (nearly) exact solution

$$\Psi_n = \left((-1)^n - \epsilon^2 V_n(X,Y) \right) y. \tag{33}$$

This is not an exact solution to (1), but we may think of it as arising due to a balance of unwritten damping and driving terms in the equation.

We again consider the quasi-geostrophic potential vorticity equations as given in the abstract form (6). We further assume that the solutions depend only weakly on the transverse, y, direction through a scaled variable $Y = \epsilon y$. We therefore write, as a generalization of (6),

$$\left(\mathcal{L} \left(-i\frac{\partial}{\partial x}, i\frac{\partial}{\partial t} \right) + \epsilon^2 \mathcal{L}^Y \frac{\partial^2}{\partial Y^2} \right) \vec{\phi} + \mathcal{B} \left(\vec{\phi}, \vec{\phi} \right) + \epsilon^2 \mathcal{M} \left(\frac{\partial}{\partial t}, \frac{\partial}{\partial x}; \epsilon x, \epsilon y \right) \vec{\phi} = 0, \tag{34}$$

where, for the quasi-geostrophic equations with shear flow as given in (33),

$$\hat{\mathcal{M}} = ik \begin{bmatrix} -V_1 k^2 - V_2 & V_1 \\ V_2 & -V_2 k^2 - V_1 \end{bmatrix}$$

and

$$\hat{\mathcal{L}}^Y = i \begin{bmatrix} k - \omega & 0 \\ 0 & k + \omega \end{bmatrix}.$$

To study how the leading edge wave is slowly modulated by the additional terms in this equation, we develop a multiple scales expansion centered around the y-independent leading edge mode $e^{i(k^{\star}x - \omega^{\star}t)}\vec{b}$. If we assume that the solution is independent of y to leading order, then the only y-dependence in the solution will be generated by the variable coefficient term $\mathcal{M}$.

We follow the standard procedure in deriving envelope equations with one major exception: we center our asymptotic expansion on the linear fronts described in the previous section instead of on normal modes. A normal-mode expansion requires a weak instability so that the leading order term in the expansion can be approximated by a neutrally stable mode. By using the linear front, we are able to carry out the expansion for strongly unstable systems by working in the reference frame moving with the front. A major side effect of centering our expansion on these fronts is that nonlinear terms will not enter our envelope equations even if nonlinearity is present in the system. The form of the asymptotics will show that this method is applicable only if the variable coefficient term $\mathcal{M}$ satisfies certain restrictions.

We recall that a multiple scales expansion to a PDE consists of expanding both the solution and its derivatives in powers of small parameter ϵ and solving a sequence of equations at increasing powers of ϵ. The modulation equations are then derived as the result of solvability conditions for these equations, necessary to preserve the assumed ordering of the expansion. We write

$$\vec{\phi} = \epsilon \vec{\phi}^{(1)} + \epsilon^2 \vec{\phi}^{(2)} + \epsilon^3 \vec{\phi}^{(3)} + \cdots, \tag{35}$$

where $\vec{\phi}^{(1)}$ is the linear leading front, slowly modulated in space and time,

$$\vec{\phi}^{(1)} = A(\xi, Y, T_2)\vec{b}e^{i(k^*x - \omega^*t)},$$

and the first correction is given by

$$\vec{\phi}^{(2)} = \left[B(X, Y, T_1, T_2)\vec{b} + \begin{pmatrix} c(k,\omega)A_\xi \\ 0 \end{pmatrix} \right] e^{i(k^*x - \omega^*t)}$$
$$+ \vec{\phi}^{(2,1)}e^{2i(k^*x - \omega^*t)} + \vec{\phi}^{(2,2)}e^{-2\,\mathrm{Im}(k^*x - \omega^*t)} + c.c.,$$

where X, Y, and T_1 are "$\mathcal{O}(\epsilon)$" slow space and time variables, T_2 is an "$\mathcal{O}(\epsilon^2)$" slow time variable, and ξ is a slow space variable in the reference frame moving with the front. The terms $\vec{\phi}^{(2,1)}$ and $\vec{\phi}^{(2,2)}$ arise due to the nonlinearity. The result of the asymptotics derived in section 3.1 may be summarized as follows.

Asymptotic result. *If $\vec{\phi}^{(1)}$ and $\vec{\phi}^{(2)}$ are defined as above, then the correction term B is of the form $B = \Theta(X, T_1, Y)A(\xi, Y, T_2)$, and A and Θ satisfy*

(36a) $$\Theta_{T_1} + v^*\Theta_X = m(X, Y),$$

(36b) $$A_{T_2} = -\frac{i\Delta_{\tilde{k}\tilde{k}}}{2\Delta_{\tilde{\omega}}}A_{\xi\xi} + \mu A_{YY}.$$

The coefficients m and μ are given below in (45) and (46).

3.1. The leading edge perturbation expansion. In this subsection, we derive the results in (36). When the solution is sufficiently small, of order ϵ or smaller, then $\vec{\phi}^{(1)}$ will approximately satisfy the linearized equation. Since the front decays exponentially, the solution will certainly be sufficiently small for sufficiently large x.

We define slow time and space scales

$$X = \epsilon x, \quad Y = \epsilon y, \quad T_1 = \epsilon t, \text{ and } T_2 = \epsilon^2 t$$

and expand the derivatives accordingly:

$$\frac{\partial}{\partial x} \rightarrow \frac{\partial}{\partial x} + \epsilon\frac{\partial}{\partial X} \text{ and } \frac{\partial}{\partial t} \rightarrow \frac{\partial}{\partial x} + \epsilon\frac{\partial}{\partial T_1} + \epsilon^2\frac{\partial}{\partial T_2}.$$

We assume that the solution depends on y only through the slow variable Y so that

$$\frac{\partial}{\partial y} \rightarrow \epsilon\frac{\partial}{\partial Y}.$$

The leading order equation is taken to be a slow modulation of the leading edge wave,

(37) $$\vec{\phi}^{(1)} = A(X, Y, T_1, T_2)e^{i(k^*x - \omega^*t)}\vec{b} + c.c.,$$

where $c.c.$ denotes complex conjugate. Recall that we may form the matrix $\hat{\mathcal{L}}(k, \omega)$ from the relation

$$\mathcal{L}e^{i(k^*x - \omega^*t)}\vec{b} = \hat{\mathcal{L}}(k, \omega)e^{i(k^*x - \omega^*t)}\vec{b}.$$

The vector $\vec{b}$ must be in its null space, so we may without loss of generality set

$$\vec{b} = \begin{pmatrix} -\hat{\mathcal{L}}_{1,2} \\ \hat{\mathcal{L}}_{1,1} \end{pmatrix}.$$

We plug in the multiple scale ansatz and separate orders to derive a formal sequence of equations of the form

(38) $\mathcal{O}(\epsilon^1),\ \mathcal{L}\vec{\phi}^{(1)} = 0,$

(39) $\mathcal{O}(\epsilon^2),\ \mathcal{L}\vec{\phi}^{(2)} = i\left(\hat{\mathcal{L}}_k\partial_X - \hat{\mathcal{L}}_\omega\partial_{T_1}\right)\vec{\phi}^{(1)} - \mathcal{B}\left(\vec{\phi}^{(1)},\vec{\phi}^{(1)}\right),$

(40)

$$\mathcal{O}(\epsilon^3):\ \mathcal{L}\vec{\phi}^{(3)} = i\left(\hat{\mathcal{L}}_k\partial_X - \hat{\mathcal{L}}_\omega\partial T_1\right)\vec{\phi}^{(2)}$$
$$+ \frac{1}{2}\left(\hat{\mathcal{L}}_{kk}\partial_X^2 - 2\hat{\mathcal{L}}_{k\omega}\partial_X\partial_{T_1} + \hat{\mathcal{L}}_{\omega\omega}\partial_{T_1}^2\right)\vec{\phi}^{(1)}$$
$$- \left(i\hat{\mathcal{L}}_\omega\partial_{T_2} + \mathcal{M} + \mathcal{L}^Y\partial_Y^2\right)\vec{\phi}(1)$$
$$- \mathcal{B}\left(\vec{\phi}^{(1)},\vec{\phi}^{(2)}\right) - \mathcal{B}\left(\vec{\phi}^{(2)},\vec{\phi}^{(1)}\right),$$

where the derivatives of $\hat{\mathcal{L}}$ are evaluated at the point (k^*,ω^*).

We see that (39) and (40) are of the form

(41) $\mathcal{L}\vec{u} = \vec{F}.$

Thus we must solve this class of linear equations. First, we define a *resonance* as a forcing term on the right-hand side which causes the solution to grow to violate the ordering (35) for large t. (The solution $\vec{\phi}^{(1)}$ is meaningful in the reference frame moving at the leading edge velocity, so it is in this reference frame we must evaluate the asymptotic ordering.) By the Fredholm alternative, a resonance will occur if $\vec{F}$ is in the adjoint null space of $\mathcal{L}$.

Nonresonance assumption. We make the standard assumption that $\mathcal{L}$ is a dispersive operator in that $\omega''(k) \neq 0$ so that if a particular wavenumber and frequency satisfy the dispersion relation $\Delta(k,\omega) = 0$, then in general multiples of the ordered pair $(nk,n\omega)$ will not also satisfy the dispersion relation, i.e., $\Delta(nk,n\omega) \neq 0$. In fact, we will make the slightly more general assumption that terms on the right-hand side of (41) of the form $\vec{F} = \vec{F}_0 e^{i(k_1 x - \omega_1 t)}$ for $(k_1,\omega_1) \neq (k^*,\omega^*)$, which arise in the course of this expansion, satisfy $\Delta(k_1,\omega_1) \neq 0$, so that (41) is solvable. *Fortunately, for all the systems we investigate, the nonvanishing condition*

$$\Delta(k_1,\omega_1) \neq 0,\ (k_1,\omega_1) \neq (k^*,\omega^*)$$

is satisfied, and there is no resonance due to nonlinear terms.

   3.1.1. $\mathcal{O}(\epsilon^2)$. The leading order ansatz (37) solves the $\mathcal{O}(\epsilon)$ equation, so we may move to the next order. The $\mathcal{O}(\epsilon^2)$ equation then becomes

(42) $\mathcal{L}\vec{\phi}^{(2)} = i\left(A_X\hat{\mathcal{L}}_k - A_{T_1}\hat{\mathcal{L}}_\omega\right)\vec{b}e^{i\theta^*} + c.c. - \mathcal{B}\left(\vec{\phi}^{(1)},\vec{\phi}^{(1)}\right),$

where we have let $\theta^* = k^*x - \omega^*t$. It will be convenient to consider the effect of the linear and nonlinear forcing terms separately.

   Nonlinear terms. The term $\mathcal{B}(\vec{\phi}^{(1)},\vec{\phi}^{(1)})$ in (42) gives rise to terms on the right-hand side proportional to $e^{2i\theta^*}$, $e^{-2\,\mathrm{Im}\,\theta^*}$. By the above nonresonance assumption, these will give rise to terms of the same form in the expression for $\vec{\phi}^{(2)}$. In the reference frame moving with the leading edge front, these have zero growth rate so are not resonant.

Linear terms. Given the nonresonance assumption, we need consider only the linear portion of (42):

$$\mathcal{L}\vec{\phi}^{(2)} = i\left(A_X\hat{\mathcal{L}}_k - A_{T_1}\hat{\mathcal{L}}_\omega\right)e^{i\theta^*}\vec{b}.$$

The term on the right-hand side will give rise to resonances unless it is perpendicular to the adjoint null space of $\mathcal{L}$. Enforcing this normal condition gives the general solvability condition [11]. Changing independent variables to

$$\xi = X - v^*T_1, \quad \tau = T_1,$$

the amplitude A is seen to depend only on the "group velocity variable" ξ:

$$A = A(\xi, T_2) \text{ or } \partial_\tau A = 0.$$

We define for the (ξ, τ) reference frame the wavenumber and frequency

$$\tilde{k} = k \text{ and } \tilde{\omega} = \omega - v^*k.$$

A (nonunique) solution is given by $\vec{a} = (a, 0)^T$, where

$$a = \frac{iA_\xi}{\mathcal{L}_{1,1}}\left(\mathcal{L}_{1,1}\mathcal{L}'_{1,2} - \mathcal{L}'_{1,1}\mathcal{L}_{1,2}\right),$$

and primes denote derivatives with respect to $\tilde{k}$. The condition that the solution decay as $x \to \infty$ prevents us from including a constant term in the general solution. We include in our full solution an additional solution to the homogeneous equation which will be used in eliminating resonances due to the variable medium. Thus the full solution reads

$$(43) \qquad \vec{\phi}^{(2)} = \left(\begin{pmatrix} a \\ 0 \end{pmatrix} + \Theta(X, T_1)A\vec{b}\right)e^{i\theta^*} + \vec{\phi}^{(2,1)}e^{2i\theta^*} + \vec{\phi}^{(2,2)}e^{-2\,\mathrm{Im}\,\theta^*} + c.c.,$$

where the terms $\vec{\phi}^{(2,1)}$ and $\vec{\phi}^{(2,2)}$ are generated by the nonlinear forcing term $\mathcal{B}$.

3.1.2. $\mathcal{O}(\epsilon^3)$. Again we consider the linear and nonlinear terms separately.

Nonlinear terms. The terms on the right-hand side of the form $\mathcal{B}(\vec{\phi}^{(1)}, \vec{\phi}^{(2)})$ and $\mathcal{B}(\vec{\phi}^{(2)}, \vec{\phi}^{(1)})$ will lead to forcing terms that look like $e^{i3(k^*x - \omega^*t)}$ and $e^{i((k_r^* + 3ik_i^*)x - (\omega_r^* + 3i\omega_i^*)t)}$ as well as terms of the type discussed in the previous section on nonlinear terms. By the nonresonance assumption, these terms do not contribute to resonances.

We note here the effect of centering our asymptotics on the leading edge front. If the expansion had been performed for normal modes, then the imaginary parts of k^* and ω^* would be zero, and there would be a forcing term proportional to $e^{i(k^*x - \omega^*t)}$ arising due to the nonlinearity. This is precisely how the cubic nonlinearity arises when the nonlinear Schrödinger or Ginzburg–Landau equation is derived as an envelope approximation—a mechanism lacking in this wave front situation.

Linear terms. As the nonlinear terms do not in general cause resonances, the solvability condition for (40) comes entirely from the linear terms, and the ordering of the expansion is violated unless

$$(44) \quad \frac{\Delta_{\tilde{k}\tilde{k}}}{2}A_{\xi\xi} - i\Delta_{\tilde{\omega}}A_{T_2} + i\Delta_{\tilde{k}}A\Theta_X - i\Delta_{\tilde{\omega}}A\Theta_{T_1}$$

$$- \det\left[\begin{array}{c|c} 1 & \\ d & \end{array}\,\mathcal{M}\left(\begin{smallmatrix} -\mathcal{L}_{1,2} \\ \mathcal{L}_{1,1} \end{smallmatrix}\right)\right]A - \det\left[\begin{array}{c|c} 1 & \\ d & \end{array}\,\mathcal{L}^Y\left(\begin{smallmatrix} -\mathcal{L}_{1,2} \\ \mathcal{L}_{1,1} \end{smallmatrix}\right)\right]A_{YY} = 0.$$

Define

$$(45) \qquad m = i \det \begin{bmatrix} 1 \\ d \end{bmatrix} \middle| \mathcal{M} \begin{pmatrix} -\mathcal{L}_{1,2} \\ \mathcal{L}_{1,1} \end{pmatrix} \end{bmatrix} / \Delta_{\tilde{\omega}},$$

$$(46) \qquad \mu = i \det \begin{bmatrix} 1 \\ d \end{bmatrix} \middle| \mathcal{L}^Y \begin{pmatrix} -\mathcal{L}_{1,2} \\ \mathcal{L}_{1,1} \end{pmatrix} \end{bmatrix} / \Delta_{\tilde{\omega}}.$$

We may split (44) in two by taking a derivative with respect to τ, recalling that $\frac{\partial}{\partial \tau} = \frac{\partial}{\partial T_1} + v^* \frac{\partial}{\partial X}$. As $A_\tau = 0$, the remaining terms will be

$$(47) \qquad -i\Delta_{\tilde{\omega}} A \left(\frac{\partial}{\partial T_1} + v^* \frac{\partial}{\partial X} \right) (\Theta_{T_1} + v^* \Theta_X - m(X,Y)) = 0.$$

This may be integrated once to obtain

$$(48) \qquad \Theta_{T_1} + v^* \Theta_X = m(X,Y) + F(\xi,Y,T_2),$$

with constant of integration F. We may solve the Θ equation to obtain

$$(49) \qquad \Theta(\xi,Y,T_1) = \frac{1}{v^*} \int_\xi^{\xi+v^* T_1} m(\tau,Y) d\tau + T_1 F(\xi,Y,T_2).$$

This explicit formula for Θ shows that the asymptotic ordering could be violated if $m(X,Y)$ is not subject to rather stringent restrictions. In general, we may set F to be

$$(50) \qquad F(Y) = - \lim_{T_1 \to \infty} \frac{1}{v^*} \int_\xi^{\xi+v^* T_1} m(\tau,Y) d\tau,$$

which means this limit must exist for each Y in the domain considered.

We then use (48) to eliminate Θ from (44), yielding

$$(51) \qquad A_{T_2} = -\frac{i\Delta_{\tilde{k}\tilde{k}}}{2\Delta_{\tilde{\omega}}} A_{\xi\xi} + \mu A_{YY} - F(\xi,Y,T_2)A.$$

3.2. The two layer f-plane without dissipation.

The first model for which we discuss the leading edge modulation equations is the inviscid f-plane. The nondimensionalization of this model and the determination of the properties of its leading edge linear front are discussed in section 2.

The leading order linear operator is discussed in section 2.4.1. Recall that the linear part of the front is of the form

$$A \begin{pmatrix} \psi_1 \\ \psi_2 \end{pmatrix} e^{i(k^* x - \omega^* t)},$$

where the wavenumber, frequency, and velocity are given by

$$\left(k^* = 1 + i; \ \omega^* = i\sqrt{2}; \ v^* = \sqrt{2} \right).$$

To form the coefficients of the two main modulation equations described in (36), we need to compute the following quantities:

$$(52a) \quad \Delta_{\tilde{k}\tilde{k}} = -2k^4 v^2 - 16k^3 v\omega + 30\,k^4 - 4k^2 v^2 - 12k^2 \omega^2 - 16kv\omega - 24k^2 - 4\omega^2,$$

$$(52b) \quad \Delta_{\tilde{\omega}} = -2k^2 \omega(2 + k^2),$$

as well as

$$\det \left[\begin{array}{c} 1 \\ d \end{array} \middle| \mathcal{M}\left(\begin{smallmatrix} -\lambda_2 \\ \lambda_1 \end{smallmatrix} \right) \right] \text{ and } \det \left[\begin{array}{c} 1 \\ d \end{array} \middle| \mathcal{L}^Y \left(\begin{smallmatrix} -\lambda_2 \\ \lambda_1 \end{smallmatrix} \right) \right].$$

Substituting the leading edge quantities (52) into the preceding expressions yields

$$\Delta_{\tilde{k}\tilde{k}} = 16i,$$

$$\Delta_{\tilde{\omega}} = 8\sqrt{2}(1+i),$$

$$\det \left[\begin{array}{c} 1 \\ d \end{array} \middle| \mathcal{M}\left(\begin{smallmatrix} -\lambda_2 \\ \lambda_1 \end{smallmatrix} \right) \right] = 8(-1 + i(1+\sqrt{2}))(-V_1 + i(\sqrt{2}-1)V_2),$$

$$\text{and } \det \left[\begin{array}{c} 1 \\ d \end{array} \middle| \mathcal{L}^Y \left(\begin{smallmatrix} -\lambda_2 \\ \lambda_1 \end{smallmatrix} \right) \right] = -4(1-i).$$

Thus the final equations are given by

$$\Theta_{T_1} + \sqrt{2}\Theta_X = i\sqrt{2}V_B + (1-i)V_T,$$

$$A_{T_2} = \frac{(1-i)\sqrt{2}}{4}A_{\xi\xi} + \frac{\sqrt{2}}{4}A_{YY},$$

where V_T and V_B are the barotropic and baroclinic parts of the velocity, respectively, as defined in (2).

3.3. β-plane equation with Ekman drag. We are unable to perform this asymptotic expansion for the β-plane equations when $r = 0$ due to the high order real root at the leading edge. We can, however, derive amplitude equations when dissipation is included. Using the values given in (29), we derive equations of the form

$$\Theta_{T_1} + c^*\Theta_X = m^T V_T + m^B V_B,$$

$$A_{T_2} = m^\xi A_{\xi\xi} + \mu A_{YY},$$

where the coefficients are given in the following table for $\beta = 1.6$, with r as given in the table.

(53)

r	m^T	m^B	m^ξ	μ
.05	$.050 - .434i$	$.249 - .349i$	$.631 + 2.66i$	$2.97 + 1.75i$
.10	$.064 - .443i$	$.311 - .306i$	$.731 + 2.38i$	$2.82 + 2.36i$
.15	$.075 - .452i$	$.348 - .269i$	$.780 + 2.17i$	$2.50 + 2.65i$

Note the interesting fact that as the dissipation increases in the full equation, the diffusion actually decreases in the Y direction as it is enhanced in the ξ direction.

4. Numerical experiments. Next we confirm numerically the asymptotic procedure described above. That the wave moves at the selected speed and has the correct decay properties has been computed by others [7, 21]. The leading edge speed, wavenumber, and frequency have been well verified for systems such as we are studying, but the challenge in confirming the asymptotics is in resolving the exponentially decaying leading edge over several orders of magnitude. In addition, the slow time scales and long spatial scales imposed by the asymptotic problem require that the numerics be carried out on a large domain for long times. While second order methods would certainly be sufficient to verify the basic properties of the unmodulated system, accurate representation of the modulations due to the weakly varying coefficients over a long domain requires a higher order method.

4.1. Description of numerical experiments. To write a code that would implement the atmospheric wave equations to the accuracy needed would be an extremely difficult task, so we choose to validate the asymptotics on a simpler model problem–a variable coefficient complex Ginzburg–Landau equation:

$$(54) \qquad u_t = (1 + \epsilon^2\mu(\epsilon x))u - vu_x + (1 + i\beta)u_{xx} - (1 + i\gamma)|u|^2u.$$

This equation is often used as a model for the evolution of systems with weak nonlinearities and weak instability [17] and has been derived as a model for the two layer quasi-geostrophic equations by Esler [9]. The problem we solve is to set $u = 1$ at $x = 0$ with compactly supported initial conditions, allowing a wave propagate to the right.

Although our general derivation of modulation equations was performed for vector systems, a similar derivation may be done for this scalar equation. For later reference, the selected wavenumber, frequency, and velocity are

$$\left(k^* = \frac{\beta + i}{\sqrt{1 + \beta^2}}; \ \omega^* = vk^* + \beta + 2i; \ v^* = v + 2\sqrt{1 + \beta^2}\right).$$

4.2. Numerical difficulties. In order to get meaningful results from this numerical experiment, a code of higher-than-usual accuracy will be needed, especially for the spatial discretization. To see why, recall that the important terms are A and Θ, where the full solution in the leading edge is of the form

$$u \sim \epsilon A e^{i(k^*x - \omega^*t)},$$

where k^* and ω^* are complex. In order to compare theory with the numerical experiment, we must know A to several decimal places, but over the domain of computation, u decays from order one down to $O(e^{-|k|/\epsilon})$. If standard Fourier methods are used to compute the derivative, then the solution can only be resolved down to size 10^{-16} in double precision arithmetic. We instead use high order methods which are more "local" in nature, which are able to resolve the amplitude of a decaying exponential over greater distances [12].

For temporal discretization, there are two competing difficulties which lead us to our numerical method. First we have stiffness due to diffusive and dispersive terms in our PDE, which would suggest that we use an implicit method. Second, we have nonlinear terms, and we would like to avoid using implicit methods and needing to solve fully nonlinear equations at each step. We would also like to be able to use a high order method so as not to squander the accuracy of the spatial discretization.

4.3. Summary of method. Briefly, our method will consist of a "method of lines." First, we impose a spatial discretization and specify a method of computing approximate spatial derivatives. This reduces the PDE to a system of ODEs for the vector $\vec{U}(t)$, which is then solved by a suitable time stepping method.

4.4. Spatial discretization. The spatial discretization is performed by a multidomain Chebyshev collocation due to Yang and Shizgal [24]. Generally, Chebyshev methods are much more adaptable to boundary conditions than are related Fourier methods. We begin by defining the standard Chebyshev collocation method and then explain the multidomain version. On the interval $[-1, 1]$ we define the Gauss–Lobatto–Chebyshev (GLC) points:

$$(55) \qquad x_k = \cos\left(\frac{\pi(k-1)}{n}\right), \quad k = 1, \ldots, n+1.$$

Let f be a smooth function defined on $[-1, 1]$, and let $\vec{f}$ be the vector $f_k = f(x_k)$ of values at the GLC points. Then we may compute an approximate derivative as

$$f'(x_k) \approx \mathcal{D} f_k,$$

where [4]

$$\mathcal{D}_{l,j} = \begin{cases} \frac{c_l}{c_j} \frac{(-1)^{l+j}}{x_l - x_j}, & l \neq j, \\ \frac{-x_j}{2(1-x_j^2)}, & 1 \leq l = j \leq N - 1, \\ \frac{2N^2+1}{6}, & l = j = 0, \\ -\frac{2N^2+1}{6}, & l = j = N, \end{cases}$$

where $c_j = 1$ for $0 < j < N$ and $c_0 = c_N = 2$ and x_j are as defined in (55). (This comes from representing f as a sum of the first $n + 1$ Chebyshev polynomials, and such a derivative converges faster than any power of N as $N \to \infty$.)

It is not practical to implement this method over a large computational domain as $\mathcal{D}$ is a dense matrix and becomes extremely ill conditioned for large values of n. Therefore, we consider a piecewise method using overlapping subdomains as described by Yang and Shizgal in [24]. In this method, we partition the interval into overlapping subdomains of equal length so that the last two GLC points in one subdomain coincide with the first two points in the next subdomain. If we choose to partition an interval of length L into J subintervals and want to use approximating polynomials of degree N, then there will be

$$M = J(N - 2) + 2$$

total collocation points, and the length l_{sub} of the subintervals will be given by

$$l_{sub} = \frac{2L}{(J + 1) + (J - 1) \cos \frac{\pi}{N}}.$$
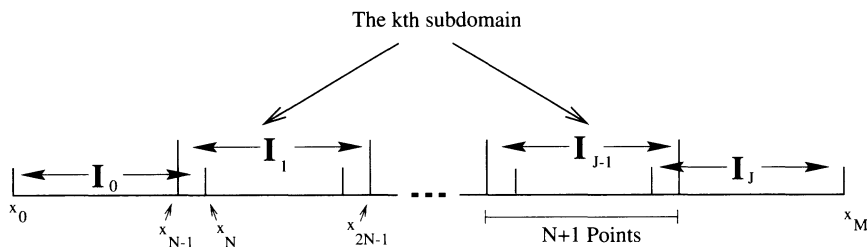
Such a partitioning is shown in Figure 4.1.

FIG. 4.1. *Partitioning of an interval into J overlapping subdomains I_k.*

If we let D be the $(N + 1) \times (N + 1)$ collocation derivative operator for a single subdomain, with the points in the subdomain labeled 0 through N, then the full operator $\mathcal{D}$ has a nearly block diagonal structure. The resulting linear system is nearly block diagonal. We may then use this approximate derivative to discretize a boundary value problem, which is very efficiently solved by Gaussian elimination using a specially adapted partial pivoting scheme, subject to the constraint that two rows may be interchanged only if they are in the same block. Such a matrix may
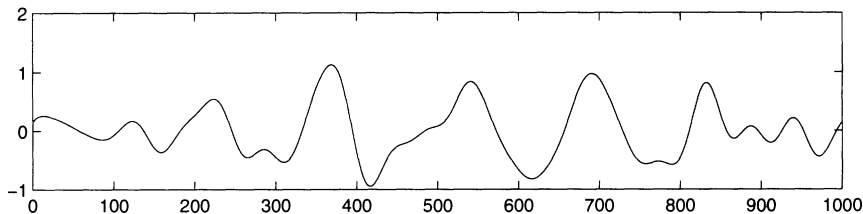
FIG. 4.2. *The variable coefficient μ used in one experiment.*

be factored in $O(JN^3)$ steps, and the forward and backward substitutions may be performed in $O(JN^2)$ steps. The elements of the matrix may be stored in a one-dimensional array, consecutively by rows, with all the arithmetic done in place with zero fill-in. Thus, with N fixed, quite large systems may be solved very efficiently. In practice $N = 6$ was found to be sufficient.

4.5. Time stepping. To solve this ODE, the right-hand side is split into two pieces: one containing all the terms responsible for stiffness and for instability and one containing all the convective and nonlinear terms. The ODE may then be written in the form

$$\dot{U} = f(U) + g(U)$$

and solved by a high order splitting algorithm described below.

The time stepping is done using the implicit-explicit multistep schemes due to Ascher, Ruuth, and Wetton [1]. These allow us to compute the nonstiff cubically nonlinear terms and advection terms explicitly, needing only to solve implicitly for the terms due to the higher order spatial derivatives. This may be thought of as a high order "splitting method," which allows us to avoid costly iterations of a nonlinear solver.

4.6. Results of one-dimensional simulations. Recall that the one-dimensional numerical experiments are performed for the model equation

$$u_t = (1 + \epsilon^2 \mu(\epsilon x))u - vu_x + (1 + i\beta)u_{xx} - (1 + i\gamma)|u|^2 u.$$

For all experiments reported, the parameters used were $v = 3$, $\beta = 1$, and $\gamma = 2$, which makes the equation convectively unstable. The experiments were performed with sixth order piecewise collocation and a total of 1000 subdomains for $0 \le x \le 1000$. A variety of variable coefficient functions $\mu(\epsilon x)$ were used, an example of which is plotted in Figure 4.2, with $\epsilon = \frac{1}{4}$. This function was generated by a random Fourier sine series. Other functions we used for μ included Gaussians, sinusoids, and sums of randomly placed Gaussians. The quality of the results was fairly independent of the shape of the variable coefficient as long as the criterion was met that the mean of μ was zero.

Figure 4.3 shows a contour plot of the wave spreading to the right at constant velocity v^*, with the variable coefficient as shown in Figure 4.2.

To postprocess these numerical results, in the parallelogram region pictured in Figure 4.3 we form $A(1 + \epsilon\Theta)$ by dividing the full solution by $e^{i(k^*x - \omega^* t)}$. This region is defined by $t_0 < t < t_1$ and $x_0 - v^* t_0 < x - v^* t < x_1 - v^* t_1$. In this region, the solution has an amplitude of about $|u| = .15$ at the left edge and about $|u| = 10^{-16}$ at the right edge due to the exponential decay of e^{ik^*x}. Thus we remove this large variation and focus on $A(1 + \epsilon\Theta)$.
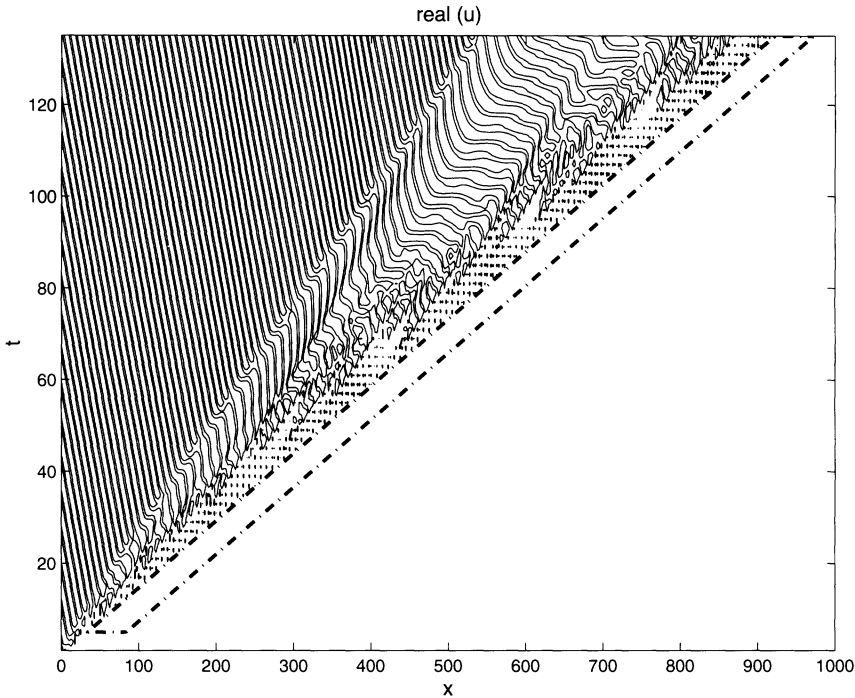
real (u)

FIG. 4.3. *Solution to the PDE spreading to the right. The parallelogram region shows the region in (ξ, T_2) variables, where the slowly varying functions A and Θ are defined.*

Next

$$\Theta(\xi, T_1) = \frac{1}{v^*} \int_{\xi}^{\xi + v^* T_1} \mu(\tau) d\tau$$

is formed from μ, where, recall, $T_1 = \epsilon t$, $\xi = \epsilon(x - v^* t)$. This allows A to be calculated from the solution to the full PDE. We may then compare its evolution with that of the envelope equation. The initial and boundary values of A are used to numerically compute the evolution of A under the reduced equation (51), and the results are compared with the values of A obtained from the full simulation. Results are shown in Figure 4.4. The relative error between the envelope A as computed from the full solution and from the asymptotic reduction is shown in Figure 4.5. Each line in the contour plot represents a one percent increment in the relative error, with a maximal relative error of about seven percent. The relative error is clearly largest at the left of the moving interval, where the solution to the PDE is largest and nonlinear effects are most important.

To show the asymptotic validity in a more quantitative manner, we run the simulation for two different values of ϵ and show that the error norm for A decreases by $o(\epsilon)$ with $\mu = \sin X$. Formally, the order of the asymptotic expansion is $O(\epsilon^3)$. In the case of scalar equations, $\vec{\phi}^{(2)}$, the $O(\epsilon^2)$ term in the asymptotic expansion (35) vanishes so that

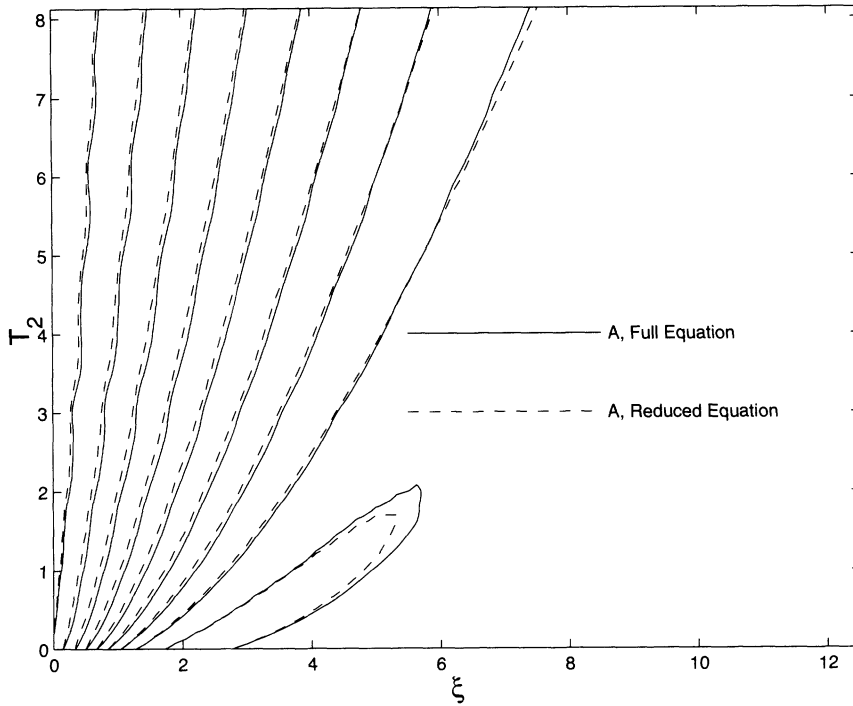$$u \sim \epsilon A (1 + \epsilon \Theta) e^{i(k^* x - \omega^* t)} + O(\epsilon^3).$$

FIG. 4.4. *The amplitude A computed from the full simulation (solid) and via the reduced equation (dotted). The contour interval for each is .1.*

Therefore,

$$\left| \frac{u}{\epsilon(1 + \epsilon\Theta)e^{i(k^*x - \omega^*t)}} - A \right| = O(\epsilon^2).$$

The error in the computed value of A at large time $t = 135$ is plotted in Figure 4.6. The empirical convergence rate, given by $\log_2 \frac{\text{Error}(\epsilon=\frac{1}{4})}{\text{Error}(\epsilon=\frac{1}{8})}$, is 1.65. While not quite $O(\epsilon^2)$, it is at least $o(\epsilon)$.

It would be useful to see if the error estimate improves as ϵ is further decreased, but it is difficult to run the numerical procedure with ϵ much smaller than $\frac{1}{8}$ because we must run the code for times of $O(\epsilon^{-2})$ on intervals of length $O(\epsilon^{-2})$ in order to compare our theory with the numerics. As the order is only exact in the limit as $\epsilon \to 0$, we may only be able to verify $o(\epsilon)$ convergence.

In section 3.1, we showed that the inhomogeneity must additionally satisfy a finite mean condition (50). We now investigate the importance of this numerically. To show that the asymptotic expansion breaks down when $\int \mu dX$ grows large, we now show an example where the order of the method begins to break down. We choose $\mu(x)$ to be a smoothed step function of height ϵ^2 and width $40/\epsilon$, and we allow the wave to propagate until it is about eighty percent of the way through the interval. We then compute the value of A by the above procedure and compare the errors when $\epsilon = \frac{1}{8}$ with those when $\epsilon = \frac{1}{4}$. The difference between the two computed values of A is
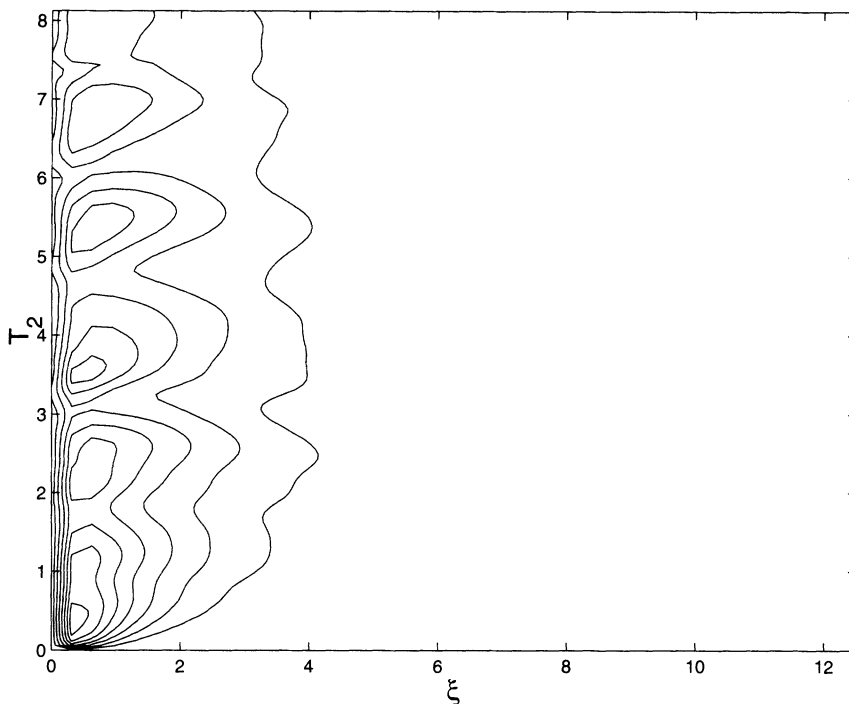
FIG. 4.5. *The relative error in A computed via two methods. Contour interval: .01; maximum relative error: .07, near left edge.*
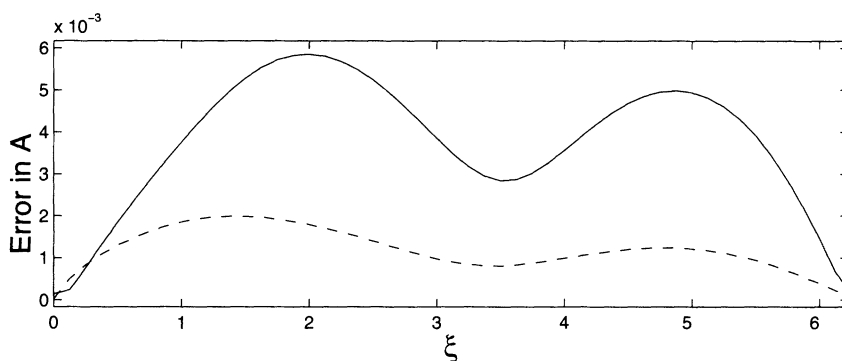

FIG. 4.6. *The difference in the amplitude A computed numerically and via the envelope equation for $\epsilon = \frac{1}{4}$ (solid) and $\epsilon = \frac{1}{8}$ (dashed), for inhomogeneity $\mu = \sin(X)$.*

shown in Figure 4.7. We compute the empirical convergence order at the final time, which is approximately 1.07, so that the convergence is approximately first order, which is a significant drop off from the previous case. This shows that the mean zero condition on the variable coefficient term (μ for complex Ginzburg–Landau, $\mathcal{M}$ for a general vector system) affects the convergence of the method and is not merely a formal breakdown in the ordering.
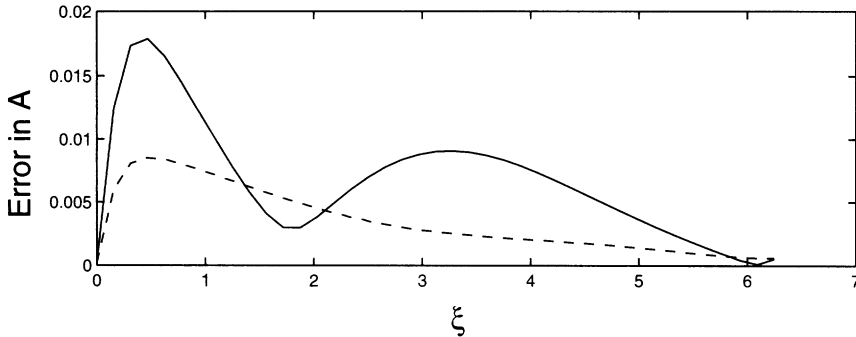
FIG. 4.7. *As in* (4.6), *with shelf-like variable coefficient.*

5. Conclusion. We have investigated a mechanism which may be responsible for downstream development in midlatitude storm tracks. We have identified linear processes in the leading edge of developing storm tracks as a possible mechanism for downstream development and applied the predictions of this theory to a two layer system of quasi-geostrophic equations which is known to exhibit downstream development.

In investigating the leading edges of unstable baroclinic waves, we have made several observations: most notably, we find that the leading edge speed changes discontinuously as the parameter β is increased from zero due to a change in the algebraic structure of the equations which determine the roots. Another interesting feature we have explored is the degenerate root in the leading edge mode of the β-plane equations and how this is regularized both by dissipation and, more interestingly, by the constraints of a finite-width channel. Studies show that in models including realistic vertical structure, the leading edge speed is actually *reduced* by the β-effect. We have also clarified some points made by Merkine [15] about the absolute instability of constant shear flow solutions of the two layer f-plane problem.

We then investigated the interaction of leading edge modes with a weakly varying medium. We generalized the standard [17] multiple scale procedure for wave packets centered on unstable normal modes to the case of wave packets centered on the wavenumber at the leading edge front. Under the scaling ansatz studied, the predominant effects are captured by linear modulation equations and are applicable only ahead of a moving front, where the solution and the nonlinear correction terms are quite small. This method was applied to derive modulation equations for the leading edges of baroclinic disturbances interacting with variable mean flows. The validity of this asymptotic representation was verified numerically on a model system of equations, and agreement was found ahead of the front, though only in regions where the solution is very small. Clearly, in order for the asymptotic representation of the leading edge to be useful, one must connect this leading edge behavior with that slightly behind the leading edge, where nonlinear effects become important.

REFERENCES

[1] U. M. ASCHER, S. J. RUUTH, AND B. T. R. WETTON, *Implicit-explicit methods for time-dependent partial differential equations*, SIAM J. Numer. Anal., 32 (1995), pp. 797–823.

[2] R. BRIGGS, *Electron Stream Interaction with Plasmas*, MIT Press, Cambridge, MA, 1964.

[3] W. S. BURNSIDE AND A. W. PANTON, *The Theory of Equations*, 8th ed., Hodges, Figgis, and Co., Dublin, 1924.

[4] C. CANUTO, M. Y. HUSSAINI, A. QUARTERONI, AND T. A. ZANG, *Spectral Methods in Fluid Dynamics*, Springer-Verlag, New York, 1988.

[5] E. K. CHANG AND I. ORLANSKI, *On the dynamics of a storm track*, J. Atmospheric Sci., 50 (1993), pp. 999–1015.

[6] E. K. M. CHANG, *Downstream development of baroclinic waves as inferred from regression analysis*, J. Atmospheric Sci., 50 (1993), pp. 2038–2053.

[7] G. DEE AND J. LANGER, *Propagating pattern selection*, Phys. Rev. Lett., 50 (1983), pp. 383–386.

[8] T. DELSOLE, *Absolute instability induced by dissipation*, J. Atmospheric Sci., 54 (1997), pp. 2586–2595.

[9] J. G. ESLER, *Wave packets in simple equilibrated baroclinic systems*, J. Atmospheric Sci., 54 (1997), pp. 2820–2849.

[10] B. F. FARRELL, *Pulse asymptotics of the Charney baroclinic instability problem*, J. Atmospheric Sci., 39 (1982), pp. 507–517.

[11] J. D. GIBBON AND M. J. MCGUINNESS, *Amplitude equations at the critical points of unstable dispersive physical systems*, Proc. Roy. Soc. London Ser. A, 377 (1981), pp. 185–219.

[12] R. H. GOODMAN, *Asymptotics for the Leading Edges of Midlatitude Storm Tracks*, Ph.D. thesis, New York University, New York, 1999.

[13] I. M. HELD AND S. LEE, *Baroclinic wave-packets in models and observations*, J. Atmospheric Sci., 50 (1993), pp. 1413–1428.

[14] P. HUERRE AND P. A. MONKEWITZ, *Local and global instabilities in spatially developing flows*, in Ann. Rev. Fluid Mech. 22, Annual Reviews, Palo Alto, CA, 1990, pp. 473–537.

[15] L. MERKINE, *Convective and absolute instability of baroclinic eddies*, Geophys. Astrophys. Fluid Dynam., 9 (1977), pp. 129–157.

[16] L. MERKINE AND M. SHAFRANEK, *The spatial and temporal evolution of localized unstable baroclinic disturbances*, Geophys. Astrophys. Fluid Dynam., 16 (1980), pp. 175–206.

[17] A. C. NEWELL, *Envelope equations*, in Nonlinear Wave Motion (Proceedings of the AMS-SIAM Summer Sem., Clarkson Coll. Tech., Potsdam, NY, 1972), Lectures in Appl. Math. 15, AMS, Providence, RI, 1974, pp. 157–163.

[18] I. ORLANSKI AND E. K. M. CHANG, *Ageostrophic geopotential fluxes in downstream and upstream development of baroclinic waves*, J. Atmospheric Sci., 50 (1993), pp. 212–225.

[19] J. PEDLOSKY, *Finite-amplitude baroclinic wave packets*, J. Atmospheric Sci., 29 (1972), pp. 680–686.

[20] J. PEDLOSKY, *Geophysical Fluid Dynamics*, 2nd ed., Springer-Verlag, New York, 1987.

[21] J. A. POWELL, A. C. NEWELL, AND C. K. R. T. JONES, *Competition between generic and nongeneric fronts in envelope equations*, Phys. Rev. A (3), 44 (1991), pp. 3636–3652.

[22] A. J. SIMMONS AND B. J. HOSKINS, *The downstream and upstream development of unstable baroclinic waves*, J. Atmospheric Sci., 36 (1979), pp. 1239–1254.

[23] K. L. SWANSON AND R. T. PIERREHUMBERT, *Nonlinear wave packet evolution on a baroclinically unstable jet*, J. Atmospheric Sci., 51 (1994), pp. 384–396.

[24] H. H. YANG AND B. SHIZGAL, *Chebyshev pseudospectral multi-domain technique for viscous flow calculation*, Comput. Methods Appl. Mech. Engrg., 118 (1994), pp. 47–61.